

Optical Properties of Radio-selected Narrow Line Seyfert 1 GalaxiesD. J. Whalen^{1,2}, S. A. Laurent-Muehleisen¹, E. C. Moran³, R. H. Becker^{1,2}**ABSTRACT**

We present results from the analysis of the optical spectra of 47 radio-selected narrow-line Seyfert 1 galaxies (NLS1s). These objects are a subset of the First Bright Quasar Survey (FBQS) and were initially detected at 20 cm (flux density limit ~ 1 mJy) in the VLA FIRST Survey. We run Spearman rank correlation tests on several sets of parameters and conclude that, except for their radio properties, radio-selected NLS1 galaxies do not exhibit significant differences from traditional NLS1 galaxies. Our results are also in agreement with previous studies suggesting that NLS1 galaxies have small black hole masses that are accreting very close to the Eddington rate. We have found 16 new radio-loud NLS1 galaxies, which increases the number of known radio-loud NLS1 galaxies by a factor of ~ 5 .

Subject headings: galaxies: Seyfert – quasars: emission lines

1. Introduction

Narrow line Seyfert 1 galaxies (hereafter NLS1s) are a class of Active Galactic Nuclei (AGN) which, like Seyfert 1 galaxies, exhibit both permitted and forbidden optical emission lines. Unlike standard broad-line Seyfert 1 galaxies, NLS1 galaxies additionally exhibit the following observational properties (Goodrich 1989): (1) the FWHM of the $H\beta$ line is less than 2000 km s^{-1} , (2) permitted lines are only slightly broader than the forbidden lines, (3) the forbidden-line emission is relatively weak, i.e., $[\text{OIII}]\lambda 5007 / H\beta < 3$, and (4) FeII and other high ionization emission line complexes are unusually strong, i.e., stronger than “normal” Seyferts, especially in the 4500–4680 Å and 5105–5395 Å wavelength ranges (Osterbrock & Pogge 1985).

It is not well understood at present what mechanism drives these differences between normal broad-lined Seyfert 1 and NLS1 galaxies. Two opposing models exist, each with their own successes

¹Department of Physics, University of California, One Shields Avenue, Davis, CA 95616; jwhalen@igpp.ucllnl.org

²IGPP, L-413, Lawrence Livermore National Laboratory, Livermore, CA 94550; bob@igpp.ucllnl.org, slaur@igpp.ucllnl.org

³Department of Astronomy, Wesleyan University, Middleton, CT, 06459; ecm@astro.wesleyan.edu

and shortcomings. The first model suggests NLS1 galaxies are viewed with the accretion disk in a face-on orientation. This case is similar to the Unified Model explanation for Seyfert 1 galaxies, with the crucial difference being that the emission lines appear narrower than typical Seyfert 1 galaxies because the optical line emitting clouds are primarily confined to a disk perpendicular to the symmetry axis, reducing the velocity dispersion along the line of sight (Osterbrock & Pogge 1985; Goodrich 1989; Puchnarewicz et al. 1992; Boller et al. 1996). The appearance of strong FeII emission could also be explained by a pole-on geometry if the FeII emission originates in the accretion disk as has been suggested by Fabian et al. (1989).

It has been alternatively proposed that the unique properties exhibited by NLS1 galaxies are a result of having accretion rates much closer to the Eddington limit than “normal” broad-line Seyfert galaxies (Laor et al. 1997). Assuming that the efficiency of conversion of accretion energy to radiation is the same in both near- and sub-Eddington sources, those sources accreting near the Eddington rate (NLS1s) should contain smaller mass black holes compared to sub-Eddington sources of the same luminosity. Smaller mass black holes in NLS1 galaxies would lead to narrower optical emission lines if the motion of the BLR region clouds are dominated by Keplerian velocities. This model also provides an explanation for many other peculiar properties of the NLS1 galaxies. For example, when the accretion rate approaches Eddington, the disk is likely “puffed up” by radiation pressure. This would result in a larger X-ray-heated volume that can (a) generate the observed FeII emission and (b) shield the NLR from UV ionizing radiation, resulting in weaker [OIII] emission.

Additional fuel which favors the accretion rate model, is provided by the work of Boroson & Green (1992). They measured many continuum and line properties for a variety of AGN and examined various correlations and inverse correlations between myriad parameters. They then reduced this large set of data to a few principal components, eigenvectors of the correlation matrix. The most important eigenvector is principal component 1 (PC1) which links the strength of FeII emission, [OIII] emission, and $H\beta$ line asymmetry, but is dominated by the inverse correlation between the strengths of FeII and [OIII]. The most popular interpretation for what PC1 physically represents is a sequence in L/L_{Edd} , the Eddington ratio. The idea is that the vertical structure of the accretion disk, governed by the Eddington ratio, drives line strengths and continuum components through its illumination of broad-line clouds and an extended narrow-line region. NLS1 galaxies lie at one extreme of the PC1 correlation (strong FeII / weak [OIII]), lending support to the idea that near Eddington accretion rates (around small mass black holes) ultimately determine whether an object manifests itself as a NLS1 or Seyfert 1 galaxy.

But more than optical emission line properties distinguish NLS1 galaxies from other classes of AGN; their X-ray properties also show marked differences compared to other types of Seyfert galaxies. The best known X-ray property of NLS1 galaxies is the presence of a soft X-ray excess (Brandt et al. 1994). NLS1 galaxies also exhibit unusually strong X-ray variability (Boller 1997; Leighly 1999). Finally, NLS1 galaxies are known to generally exhibit steeper hard (2-10 keV) X-ray spectra than broad-line Seyfert 1 galaxies (Brandt, Mathur & Elvis 1997).

Most of these X-ray properties can be explained within the framework of either the orientation or accretion-rate models, although each requires some special assumptions or modifications. Within the general confines of the orientation model, Madau (1988) has examined the properties of geometrically thick accretion disks and predicts a strong soft X-ray emission when these disks are viewed face-on. In the accretion-rate models, the observed soft excesses in NLS1 galaxies is attributed to thermal emission from a viscously heated accretion disk that results at an accretion rate close to the Eddington limit (Pounds, Done & Osborne 1995). Likewise, enhanced variability in NLS1 galaxies can be explained via either the orientation or accretion rate models. If NLS1 galaxies do accrete near Eddington and have smaller mass black holes, their size scale is smaller and the variability can be more rapid. In the orientation model, the variability may be enhanced via relativistic boosting of the emission.

The trend toward harder spectra in normal broad-lined Seyfert galaxies is the one observational characteristic which is difficult to explain in the orientation model. In this model, the hard photon index is expected to become softer as the inclination angle increases (Haardt & Maraschi 1993), the opposite of which must be true for this model to explain differences seen between NLS1 and normal Seyfert 1 galaxies. However, when this model is generalized, and the hot phase is assumed to be in localized regions on the disk, the dependence on inclination decreases, and the index depends rather on the height of the hot phase blobs above the disk. In this case, there is a need to invoke a mechanism which links the height of sites which produce the bulk of the observed emission with orientation in order to fit within the orientation based scheme. This is a difficult proposition without invoking some ad hoc physical structure that reflects or absorbs radiation asymmetrically. In the high accretion rate model, however, the steeper hard X-ray spectrum of NLS1 galaxies can be explained if the hot phase luminosity is smaller in NLS1 galaxies, presumably due to the smaller central black hole mass.

Despite years of work, both the orientation and accretion rate models are still essentially equally viable; both provide a framework which unifies NLS1 galaxies and normal Seyfert 1 galaxies, yet neither is entirely satisfactory. Additional observational constraints would go a long way toward resolving the question. Radio observations may well provide those constraints; they have undoubtedly been crucial in the formulation of unification scenarios for other classes of AGN. But while Seyferts of all types have been studied extensively at optical and X-ray wavebands, little is known about the radio properties of NLS1 galaxies in part because they are typically faint radio sources, if they are known to be radio sources at all. One of the few systematic studies of the radio properties of NLS1 galaxies is by Ulvestad et al. (1995). They observed a group of 15 NLS1 galaxies (of which only 9 were detected in radio) and found relatively modest radio powers for their sample (10^{27} - 10^{30} erg s⁻¹ Hz⁻¹). These 15 NLS1 galaxies were all radio quiet, i.e., the ratio of radio luminosity to optical luminosity is relatively small. Moran et al. (2003) show in their study that NLS1 galaxies can be radio intermediate and even radio luminous, and, as a whole, are more radio luminous than classical Seyferts.

The work of Ulvestad et al. (1995) is a radio study of optically selected NLS1 galaxies while

the Moran et al. (2003) work is a radio study of X-ray and IR selected NLS1 galaxies. There are no studies of a radio-selected sample of NLS1 galaxies. This is partly because only recently has it become apparent that NLS1 galaxies can exhibit significant radio luminosities (Siebert et al. 1999; Gliozzi et al. 2001; Oshlack, Webster & Whiting 2001). Additionally, it is only recently that new radio surveys have emerged which cover a wide area of sky to depths of only a few mJy. It is from one such survey, the FIRST (Faint Images of the Sky at Twenty Centimeters; Becker et al. (1995)) that we have compiled the first known sample of radio-selected NLS1 galaxies, and in the process increased by a factor of five the number of known radio-loud NLS1 galaxies.

In this paper we present 47 NLS1 galaxies along with 15 BLS1 galaxies with very narrow lines selected from FIRST and analyze their optical and radio properties. We will use an $H_0 = 65 \text{ km s}^{-1}$, $\Omega_{matter} = 0.3$, $\Omega_{\Lambda} = 0.7$ cosmology throughout.

The structure of this paper is as follows: In sections 2 and 3 we describe the sample selection criteria. In section 4 and 5 we describe the data and the data analysis and in section 6 the method we use for estimating central black hole mass is explained. We present our results and correlations in Section 7 and discuss the radio properties in section 8. The conclusion follows in section 9.

2. The Sample

Our objects were initially selected from the FIRST radio survey which at the time (Feb. 1999) covered ~ 2700 square degrees of the sky centered on the North Galactic Cap, and is sensitive down to a flux density limit of $\sim 1 \text{ mJy}$ at a wavelength of 20 cm. The FIRST survey was carried out with the VLA in the B-configuration and has a 5 arcsecond resolution.

The present sample of NLS1 galaxies is a subset of the larger FIRST Bright Quasar Survey (FBQS) and therefore shares many of the FBQS selection criteria, the details of which can be found in White et al. (2000). Briefly, the digitized Palomar Observatory Sky Survey (POSS) was searched for optical counterparts within 1.2 arcseconds of FIRST radio sources. If the optical counterpart existed and was classified as stellar by the Automated Plate Machine (APM) on either the red (E) or blue (O) plates, the object became an FBQS candidate. Objects brighter than 17.8 mag on the E-plate (using re-calibrated, extinction corrected magnitudes), with colors bluer than $(O - E) = 2$ were selected for spectroscopic followup observations. Optical spectroscopy was then performed on over 1,200 candidates.

Among the many quasars, low luminosity AGN, starburst and “normal” galaxies in the original FBQS study, 45 objects were selected as possible NLS1 galaxy candidates. An additional 17 objects were obtained from various followup programs to the FBQS, including the partially complete (at the time) “zero declination” strip, a small multiply-observed (in the radio) area of sky centered at zero degrees declination and extending from approximately 21 hours to 3 hours of right ascension. Only the initial 45 objects are from a spatially complete sample, having been selected as part of the original 2,700 square degree survey. All objects do, however, satisfy the above criteria.

The sample of 62 NLS1 and BLS1 galaxies has a redshift range extending from $z = 0.065$ to 0.715. The distribution of redshifts for all 62 galaxies is shown in Figure 1. Due to the fact that these objects were primarily identified by $H\beta$ FWHM and [OIII] properties, one would not expect to find objects of much greater redshift in this sample, as the $H\beta$ and [OIII] lines would be redshifted out of the optical wavelength range.

We note that one NLS1 galaxy in our sample, 0833+5124, actually violates one of the FBQS selection criterion, having an extinction corrected E-magnitude of 17.85. We nevertheless include it here, since we intend to find NLS1 galaxies with radio emission. We additionally point out that many of our spectra have $\text{FWHM}(H\beta) > 2000 \text{ km s}^{-1}$. In the original definition for NLS1 galaxies (Osterbrock & Pogge 1985), the criteria for line width was simply that the permitted lines were only slightly broader than forbidden lines. We have decided to include these galaxies as we can investigate these transition objects along with our NLS1 galaxies. We shall refer to these objects as Broad Line Seyfert 1 galaxies (BLS1s) consistently. None of these objects have very broad lines, the largest being $\sim 3000 \text{ km s}^{-1}$ full width at half maximum. However, these transition objects shall always be clearly marked in the figures and any correlations will be run both with and without these transition objects.

We also note that this sample should *not* be viewed as a complete sample of radio-selected NLS1 galaxies, since the inclusion in the FBQS requires the optical counterparts be unresolved and not very red; clearly these criteria select against Seyfert type galaxies. Nevertheless, significant numbers of Type 1, 2, Narrow-line Seyfert and starburst galaxies are present in the FBQS. This is because (1) the morphology classification from the APM plates are not precise and (2) the FBQS selection criteria erred on the side of caution, excluding only *obviously* resolved and/or red objects. Still, our sample of NLS1 galaxies is incomplete with respect to a purely radio-selected NLS1 sample, but will provide a useful comparison between the class properties of optical- vs. radio-selected NLS1 galaxies.

This comparison is particularly enlightening since PC1 tends to also trace degrees of radio-loudnesses (ratio of radio to optical flux). Objects that have strong FeII and weak [OIII] also tend to be radio-quiet and to have $H\beta$ lines that are narrower; objects that have weak FeII and strong [OIII] tend to be radio-loud and to have $H\beta$ lines that are broader. Narrow-line Seyfert 1 galaxies, therefore are expected to be radio-quiet (and usually are). However, by selecting our sample from FIRST, we favor finding radio-loud objects which most strain the PC1 correlation. In fact, many of the 47 narrow line Seyfert 1 galaxies in our sample are radio-loud, some remarkably so (See section 5). While it is not surprising we have found some radio-loud NLS1 galaxies, it is interesting that we have found enough to increase by a factor of five the number of known radio-loud NLS1 galaxies. These objects in particular should test the competing merits of the orientation vs. accretion-rate models.

3. NLS1/BLS1 Cut

In this section we address which objects should be considered NLS1 galaxies, and which should be standard Seyfert 1 galaxies, which we will refer to as BLS1s as mentioned previously. An example of each is shown in Figure 2. How should we make the cut? The criteria of Goodrich (1989) state that $\text{FWHM}(\text{H}\beta)$ should be less than 2000 km s^{-1} , but Osterbrock & Pogge’s 1985 criteria were simply that $\text{FWHM}(\text{H}\beta)$ only slightly greater than the width of the forbidden lines. As the attentive reader may have noticed, some of our objects have a $\text{FWHM}(\text{H}\beta) > 2000 \text{ km s}^{-1}$. Why do we include these? These objects have $\text{FWHM}(\text{H}\beta)$ whose widths are not much greater than the $\text{FWHM}([\text{OIII}])$ as we can be seen in Figure 3. In this figure we plot the ratio $\text{FWHM}(\text{H}\beta)/\text{FWHM}([\text{OIII}])$ against $\text{FWHM}(\text{H}\beta)$. When we compare the objects less than 2000 km s^{-1} and greater than 2000 km s^{-1} , there is little difference. Other than the two objects whose ratio is ~ 4 at about 2500 km s^{-1} , the objects whose $\text{FWHM}(\text{H}\beta)$ are greater than 2000 km s^{-1} are not unusual. Considering that these objects satisfy NLS1 criteria in all other ways, ($[\text{OIII}]/\text{H}\beta < 3$, significant FeII complexes, small black hole mass), it doesn’t seem unreasonable to call these objects NLS1 galaxies. We shall not be taking such a bold step, however, and will simply refer to objects with $\text{H}\beta > 2000 \text{ km s}^{-1}$ as Broad Line Seyfert 1 galaxies, or BLS1s. Objects with $\text{H}\beta < 2000 \text{ km s}^{-1}$ will be labelled NLS1s, and are the traditional narrow-line Seyfert 1 galaxies. X-ray data on these objects could define where the physical break between NLS1s and BLS1s should be, if it exists.

4. The Data

Once FBQS targets were identified, spectra of the candidate quasars were taken at several different sites and of the initial ~ 1200 point sources in the FBQS (White et al. 2000), ~ 600 were classified as starburst galaxies with the rest being classified as Active Galactic Nuclei (AGN). The NLS1 candidates were chosen through visual inspection and then confirmed using the above criteria, i.e., $\text{H}\beta$ FWHM similar to forbidden lines, FeII emission was present, and $[\text{OIII}]/\text{H}\beta < 3$. The spectra of all 62 objects can be found in the FBQS papers, Gregg, Becker & White (1996) and White et al. (2000).

Six observatories were used to obtain the spectra. The telescopes and instruments and the respective instrumental resolutions appear in Table 1. The observations were made under a wide variety of conditions, from photometric to cloudy, with both good and bad seeing. Many of the objects were observed twice. The spectral data were reduced using standard long slit spectral reduction packages in IRAF.

5. Analysis

The reduced data were fit using the SPECIFY routine in the IRAF (v.2.11.3) data analysis program. The broad permitted lines of the FeII complexes commonly found in NLS1 galaxies can severely contaminate the spectrum and make accurate measurements of fluxes and line widths difficult. In an effort to increase the accuracy of the line profiles, the FeII complexes were subtracted from the data before measurement of the other quantities. We used the method of Boroson & Green (1992) to remove the FeII complexes, a brief description of which follows.

The FeII complexes from the spectrum of I Zw 1 were used to create a template for use in modeling the FeII emission of other NLS1, the same procedure and template used by Boroson & Green(1992). The FeII template has spectral coverage extending from $\lambda 4250 \text{ \AA}$ to $\lambda 5700 \text{ \AA}$. We varied the amplitude of the template and also Doppler broadened the line profile until we were able to fit the observed FeII lines. We then subtracted the FeII contribution to our spectra. All data were de-redshifted to the rest frame before being fit.

The $H\alpha$, $H\beta$, and $H\gamma$ emission lines were fit both with a Lorentzian profile and a Gaussian profile. We observed that the Gaussian profile missed the broad wings of the hydrogen lines, confirming previous results (i.e., Veron-Cetty et al. (2001) and references therein). The flux, FWHM and equivalent width of each line was measured. The [OIII] $\lambda 5007$ and [OIII] $\lambda 4959$ forbidden lines were fit using a Gaussian line profile. The FWHM for the emission lines $H\beta$, [OIII] $\lambda 5007$, and [OIII] $\lambda 4959$ for each source were measured. All line profiles have been corrected for instrumental broadening, using the instrumental resolution calculated by White et al. (2000), for which the authors used calibration lamp lines to determine the broadening. These quantities are tabulated in Table 2 with the exception of [OIII] $\lambda 4959$ whose FWHM and flux were forced to follow [OIII] $\lambda 5007$, i.e., the FWHM is the same and the flux is one third the [OIII] $\lambda 5007$ value. Three objects, 1421+2824, 1644+2619, and 2155–0922, have sky absorption lines that eliminated significant parts of the [OIII] $\lambda 5007$ line. We were unable to accurate measurements of these three lines due to their destruction by the sky lines. [OIII] $\lambda 4959$ was either too small or also affected by the sky lines to use as an estimate. The three cases are noted in Table 2. The continuum portion of the spectrum was fit with a power law ($F_\lambda \propto \lambda^{-\alpha}$). The optical continuum slopes are defined between 3000 \AA and 7000 \AA and the distribution of optical continuum slopes, α , is shown in Figure 4.

The observing conditions were not necessarily photometric and therefore we restrict the bulk of our analysis mainly to quantities that are not dependent on absolute flux scale. Equivalent widths for the emission lines were calculated using the measured integrated flux from SPECIFY and dividing by the continuum strength at the center of the line using the power law model fit that SPECIFY produced. To get an equivalent width for the FeII continuum, we restricted our attention to two portions of each individual spectrum. The section between 4434 \AA and 4684 \AA and from 5147 \AA to 5350 \AA was used except in the case of 1256+3852. For this object we considered the blue section only as the wavelength coverage was not great enough to reach the red section. The $H\beta$, [OIII] $\lambda 5007$, [OIII] $\lambda 4959$, and $H\gamma$ emission lines were subtracted and the remaining spectra

were normalized by the continuum. We then integrated the FeII spectrum over the two sections to get the equivalent width of the entire FeII complex (see Table 2).

The k-corrected radio loudness parameter, R^* , was calculated for each object using the formulas (Stocke et al. 1992),

$$\log f(5 \text{ GHz}) = -29.0 + \log S_\nu + \alpha_\nu \log [5/\nu] - (1 + \alpha_\nu) \log (1 + z), \quad (1)$$

$$\log f(2500\text{\AA}) = -22.38 - 0.4B + (1 - \alpha_\lambda) \log(1 + z) + (2 - \alpha_\lambda) \log\left(\frac{2500\text{\AA}}{4409\text{\AA}}\right), \quad (2)$$

$$\log R^* = \log f(5 \text{ GHz}) - \log f(2500\text{\AA}). \quad (3)$$

In Equation 1 above, $f(5\text{GHz})$ refers to the 5GHz (6cm) flux, S_ν is the flux of frequency ν , and ν is the frequency in units of GHz. The symbol α_ν is the slope of the radio continuum such that $S_\nu \propto \nu^\alpha$ and z is the object’s redshift. In Equation 2 $f(2500\text{\AA})$ is the rest frame flux at 2500Å, z is the redshift, B is the Johnson B-band magnitude, and α_λ is the slope of the optical continuum where $F_\lambda \propto \lambda^{-\alpha}$. Formula 2 has been altered from the version in Stocke et al. (1992). That formula had no optical slope variable, α_λ . Instead, a slope of $\alpha_\lambda = -1$ (in our form of the equation) was assumed and hard-wired into the formula. We have measured optical slope as part of our analysis so we followed Schmidt (1968), Wills & Lynds (1978), and Sramek & Weedman (1980), and put the optical slope variable back into the equation. We follow the procedure laid out in White et al. (2000) and substitute O magnitudes from POSS I for Johnson B-band magnitudes.

A histogram of the optical slope data, gathered in bins of size 0.20 is shown in Figure 4, with the radio loud objects being the shaded part of the distribution. We use Formula 2 instead of simply getting the 2500Å flux from our spectra for two reasons. The first reason is that all of our objects have O magnitudes while not all of the spectra have the coverage to reach 2500 Å. The second is that the POSS magnitudes have been recalibrated plate by plate using magnitudes from the Minnesota Automated Plate Scanner POSS-I catalog and carefully corrected for extinction by the FBQS team (White et al. (2000) and references therein), while our spectra are not assumed to be photometric and therefore not as useful for calculation requiring absolute flux scale measurements. The extinction corrected O magnitudes will be more accurate.

The k-corrected radio loudness parameter R^* , as shown in Equation 3, is the ratio of radio flux to optical flux. AGN are often described as radio-loud or radio-quiet depending on the value of this ratio. In terms of the R^* parameter radio-loud objects have the value $R^* \geq 10$ ($\log R^* \geq 1$) and radio-quiet objects have values of $R^* \leq 1$ ($\log R^* \leq 0$). NLS1 galaxies have traditionally been found to be radio-quiet.

We found that only three of the objects have published radio data in other useful wavelengths. We used data from the Green Bank 6 cm radio survey to calculate the slopes for those three objects

but we assumed a slope of $\alpha_{radio} = -0.5$ in the form $S_\nu \propto \nu^{\alpha_{radio}}$ for the rest of the sample. This is the slope that was used by Ho & Peng (2001) in their study of the radio properties of Seyfert 1 nuclei. It is possible that we are underestimating the number of radio loud sources in our sample.

6. Estimating the Black Hole Masses

Recent papers have investigated the possibility that the unusual spectral properties of NLS1 galaxies can be explained by assuming an accretion rate close to Eddington and a small black hole mass. A small black hole mass accreting efficiently could explain narrow permitted line widths (by way of smaller Keplerian velocities) and lower radio luminosities (assuming the black hole powers radio emission). We estimate black hole masses of our sample using recent techniques to test whether or not our data fits this paradigm.

To estimate the black hole masses we use the method of McLure & Dunlop (2002) which utilizes the FWHM(H β) and 5100 Å luminosity as surrogates for black hole mass. As mentioned previously, our spectra are not necessarily photometric, so they needed to be corrected before using this formula to estimate black hole mass. We used the POSS E and O magnitudes along with the IRAF package SYNPHOT to calibrate our spectra and find the appropriate correction factor. Briefly, armed with the transmission curve for POSS E and O plates, we send our spectra through the model O and E filters and calculate the the O and E magnitudes using SYNPHOT. We use the difference between these synthetic magnitudes and the measured, photometric magnitudes from the actual POSS plates to find the flux difference via $\Delta m \propto \log(\frac{f_1}{f_2})$. The correction is applied and the corrected flux used to determine L_{5100} .

The formula we used is the following from Grupe & Mathur (2004):

$$\log M_{BH} = 5.17 + \log R_{BLR} + 2[\log \text{FWHM}(\text{H}\beta) - 3] \quad (4)$$

where

$$\log R_{BLR} = 1.52 + 0.70(\log \lambda L_{5100} - 37). \quad (5)$$

Here M_{BH} is the black hole mass in units of solar mass, M_\odot , R_{BLR} is the radius of the broad line region in light-days, and λL_{5100} is the rest frame monochromatic luminosity at 5100 Å in Watts. Figure 5 shows the distribution of black hole masses for our sample, with the NLS1 galaxies being represented by the shaded parts of the histogram. These masses are small for typical AGN.

Recent work by Grupe & Mathur (2004) and Mathur et al. (2001) suggests that NLS1 galaxies may be AGN in an early stage of AGN development. In this scenario, NLS1 galaxies have small black hole masses that steadily grow by accretion in well formed bulges. To illustrate this claim, the $M_{BH} - \sigma$ relation which is the tight correlation between central black hole mass and bulge mass

found by Gebhardt et al. (2000), Ferrarese & Merrit (2000) among others, is applied. The stellar velocity dispersion, which is used to measure the bulge mass, can be estimated using $\text{FWHM}([\text{OIII}])$ as was found in Boroson (2003) and references therein. Using the above formula for M_{BH} and $\text{FWHM}([\text{OIII}])$ as a surrogate for stellar velocity dispersion, the $M_{BH} - \sigma$ relation for NLS1 galaxies was plotted. In their 2004 paper, Grupe & Mathur applied this method to an X-ray selected sample of NLS1 galaxies and reported that the sample had both small black hole masses and that the galaxies fall below the empirical line found by Tremaine et al. (2002) for normal galaxies. They conclude that NLS1 galaxies do not follow the $M_{BH} - \sigma$ relation. As can be seen in Figure 6, although our data are radio selected as opposed to X-ray selected, the radio selected NLS1 galaxies follow the same trend. Our NLS1 galaxies appear to have fairly small black hole masses and do not closely follow the black hole mass-bulge mass relation.

7. Results and Correlations

In this section we will calculate several parameters relevant to NLS1 study, test for correlations between sets of parameters, and then compare with other published results. We run correlation tests with several different cuts. Once with all objects in our sample included, once with the BLS1 galaxies ($\text{FWHM}(\text{H}\beta) > 2000 \text{ km s}^{-1}$) removed, and on each of the previous samples with radio loud and radio quiet points considered separately. We use the Spearman rank correlation test because it is less sensitive to the occasional extreme data point.

7.1. $\text{EW}(\text{FeII})$ vs. $\text{EW}([\text{OIII}])$

Boroson & Green (1992) find that PC1 is driven by an anti-correlation between the strengths of the iron complexes and the strengths of the $[\text{OIII}]\lambda 5007$ line. We check in Figure 7 for the same correlation in our sample. For our sample we find a very weak borderline anti-correlation ($\rho_{\text{Spearman}} = -0.250$, $P = 0.064$). These correlations were performed on only 56 pairs of points as three of the objects did not have measureable FeII and another three had $[\text{OIII}]$ lines eliminated by atmospheric absorption. When the test is performed on only the NLS1 objects, the anti-correlation non-existent, with $\rho_{\text{Spearman}} = -0.243$ and $P = 0.119$. The trend found by Boroson & Green for low redshift quasars is not found in our sample of NLS1 galaxies. However, it is the case that, in general, this sample has fairly weak $[\text{OIII}]$ emission and strong FeII.

7.2. $\text{EW}([\text{OIII}])$ vs. $\text{FWHM}(\text{H}\beta)$

In Boroson & Green’s analysis they find that while PC1 is driven by the anti-correlation between the strength of the FeII and $[\text{OIII}]$ lines, they also find that the equivalent width of $[\text{OIII}]$ and $\text{FWHM}(\text{H}\beta)$ increase with PC1 and, therefore, are at least weakly correlated. We test

this possibility on the present sample in Figure 8, where we plot the logarithm of $\text{EW}([\text{OIII}])$ against $\log \text{FWHM}(\text{H}\beta)$. Our result does not confirm this statement as there appears to be no correlation between the two. Applying the Spearman rank correlation test we get $\rho_{\text{Spearman}} = 0.045$ corresponding to a probability of chance correlation of $P = 0.73$ using a total of 59 data points. When we remove all the objects with corrected $\text{FWHM}(\text{H}\beta) > 2000 \text{ km s}^{-1}$ (leaving a total of 44 objects) and run the Spearman test again we get $\rho_{\text{Spearman}} = 0.040$ corresponding to a probability of $P = 0.795$, i.e., these parameters are uncorrelated. The correlation between these two parameters seen by Boroson & Green is not present in our sample.

7.3. $\text{EW}(\text{FeII})$ vs. $[\text{OIII}]/\text{H}\beta$ ratio

In Figure 9 we plot FeII equivalent width versus the $[\text{OIII}]/\text{H}\beta$ ratio. The $[\text{OIII}]/\text{H}\beta$ always refers to the ratio of the integrated rest-frame fluxes throughout this paper. Here there is a significant anti-correlation with a spearman rank correlation coefficient of $\rho_{\text{Spearman}} = -0.388$ and a probability of chance correlation of 0.004 for 56 of the objects in our sample. Of the six objects excluded, three did not have $[\text{OIII}]$ measurements as noted earlier, and three others did not have a suitable FeII measurement. A similar result holds for the 42 NLS1 galaxies, with $\rho_{\text{Spearman}} = -0.419$ and $P = 0.007$. These are all noted in Table 2. This is in agreement with the results of Grupe et al. (1999), which considers a sample of 76 soft X-ray sources with 36 NLS1 galaxies. This result was also found in other studies (e.g., Boroson & Green (1992) and Laor et al. (1997)). Both the optically selected sample and the X-ray selected sample show the same correlations as our radio selected sample.

When the $\log R^* \geq 1$ and $\log R^* < 1$ samples are considered separately, we find that the two sub-samples differ slightly. The radio quiet ($\log R^* < 1$) sample is significantly correlated ($\rho_{\text{Spearman}} = -0.436$, $P = 0.007$), in agreement with the result for the larger sample. However, for the radio loud ($\log R^* \geq 1$) sub-sample the correlation test fails, and no correlation is present. As there were only 16 data points, and since Spearman is only accurate for $N > 30$, we used a generalized Kendall’s Tau method and got $\tau_{\text{Kendall}} = -0.367$ with a corresponding probability of $P = 0.32$. Regardless of the small number in the sub-sample, this result should be accurate to within 5%. There seems to be a significant difference in the two sub-samples. In this case, the radio loud and radio quiet NLS1 galaxies are behaving differently.

7.4. $[\text{OIII}]/\text{H}\beta$ ratio vs. optical slope

The plot of optical slope vs $[\text{OIII}]/\text{H}\beta$ ratio is shown in Figure 10. We find a significant anti-correlation here, similar to that found in Grupe et al. (1999), with a $\rho_{\text{Spearman}} = -0.345$ and a chance probability of $P = 0.009$. The correlation is equally strong when only NLS1 galaxies are considered. The $[\text{OIII}]/\text{H}\beta$ ratio decreases as the optical continuum grows steeper and more blue.

As noted in Table 2, three of our objects have both of the [OIII] lines rendered unmeasurable by atmospheric absorption.

7.5. EW(FeII) vs. $\log R^*$

It has been theorized that radio loudness can be correlated with FeII strength, as FeII emission is thought to be directly related to accretion rate. Boroson (2002) finds NLS1 galaxies at an extreme of PC1, the interpretation of which is that FeII emission is strong when radio loudness (and luminosity) is weak. This suggests the possibility that FeII emission and radio loudness are linked in some way. We plot these two quantities against one another in figure 11 and calculate the correlation strength. The result for the NLS1 galaxies is $\rho_{Spearman} = -0.078$ and random probability of 0.61. When the BLS1 objects are added to the sample, the result is the same. We do not find a correlation.

7.6. FeII/[OIII] ratio vs. $\log R^*$

Figure 12 shows the ratio of equivalent widths of the FeII complexes and [OIII] 5007 emission vs. radio loudness. Boroson & Green reported for their optically selected sample of AGN that those with stronger FeII emission and weaker [OIII] tended to be radio quiet while those with weaker FeII and stronger [OIII] radio loud, though not exclusively radio loud. Our radio selected sample of narrow and broad line Seyferts suggests the same trend, with a weak anti-correlation between FeII/[OIII] and radio loudness. Spearman’s rho for this plot is $\rho_{Spearman} = -0.254$ and probability of random correlation is 0.059. The NLS1 galaxies considered separately have $\rho_{Spearman} = -0.387$ and $P = 0.013$, which is a noticeably stronger correlation.

In figure 13 we have plotted $\log R^*$ vs. [OIII]/H β ratio. The Spearman correlation test on 44 NLS1 galaxies yields a statistically significant correlation, with $\rho_{Spearman} = 0.442$ and probability of no correlation of 0.004. There is a trend toward higher $\log R^*$ for greater [OIII]/H β ratio. When the BLS1 galaxies are added, the correlation is still fairly strong.

7.7. FWHM(H β) vs $\log R^*$ and L_{20cm}

In Figure 14 we present a plot of radio loudness vs. FWHM(H β) ($\rho_{Spearman} = -0.046$, probability = 0.72), which appears to be uncorrelated. We also test 20 cm radio luminosity plotted against FWHM(H β). The Spearman rank correlation test was run on all data points and the result was a significant correlation with $\rho_{Spearman} = 0.331$ and probability of chance correlation = 0.01. The results are shown in Figure 15. The radio loud objects have filled in symbols and the others have open symbols. While the radio loud objects are slightly more luminous in the radio than

the radio intermediate and radio quiet objects, they follow the same trend; increasing $\text{FWHM}(\text{H}\beta)$ follows increasing 20 cm radio power.

8. Radio Properties

Probably the most interesting results from the analysis of our sample are the radio properties. Until now, only 4 radio loud NLS1 galaxies have been discovered and published (Remillard et al. 1986; Grupe et al. 2000; Oshlack, Webster & Whiting 2001; Zhou et al. 2003). In our sample we have 16, increasing the total number of known radio loud NLS1 galaxies by a factor of ~ 5 . The distribution of the k-corrected radio loudness parameter, $\log R^*$, shown in Figure 16 demonstrates the singular nature of our sample. NLS1 galaxies are known to be radio quiet objects, most having little radio emission or none at all. Note that the majority of the sources are clustered between $0 < \log R^* < 1$. This distribution is typical for FIRST sources, as the survey finds many objects in the radio intermediate range. However, for a sample of NLS1 galaxies, the distribution is quite striking in that it is very radio loud. Although NLS1s are typically radio quiet, in this sample there are only a few radio quiet objects. At this point there are only ~ 350 NLS1 galaxies published, four of which are radio loud. This sample adds significantly to the number of known NLS1 galaxies and especially to the number of radio loud NLS1 galaxies.

In figure 17 we show several sample 20 centimeter radio contours of our NLS1 galaxies. All the sources show little or no structure, instead they are simply point sources. This agrees with the argument put forth by Goodrich (1989) that one possibility for the narrow permitted line profiles in NLS1 galaxies is that they are seen pole on, and that the gas motion is mainly confined to a disk. The lack of structure is interesting, although many of these objects are only a few mJy and more data are needed to confirm this result.

As stated previously, NLS1 galaxies are considered to be radio quiet and not very radio luminous. The only previous study of the radio properties of NLS1 galaxies was presented in a 1995 paper by Ulvestad et al. (1995), who looked at 15 NLS1 galaxies and detected 9 in the radio. They found radio powers of $10^{27} - 10^{30} \text{ erg s}^{-1} \text{ Hz}^{-1}$ at 20 cm and all the objects were radio quiet, i.e., $\log R^* < 0$. The distribution of 20 cm luminosities for our sample is shown in Figure 18. Our objects span the range from $10^{29} - 10^{33} \text{ erg s}^{-1} \text{ Hz}^{-1}$, again, typical for the FIRST survey but a factor of $10^2 - 10^3$ times greater than the Ulvestad study.

The Boroson & Green (1992) statistical analysis of the spectral properties of 75 optically selected quasars from the Palomar-Green survey included a small subsample of NLS1 galaxies. BG92 measured the optical emission-line properties and a broad range of continuum properties, from the X-ray through the radio, and performed a principal component analysis (PCA) on the data. The PCA produced several eigenvectors, the two most prominent being PC1 (related to Eddington ratio) and PC2 (related to accretion rate). When PC1 is plotted against PC2 their figure seems to suggest that black hole mass correlates with radio loudness. In figure 19 we consider all 62 objects in

our sample and plot black hole mass vs. radio loudness and get $\rho_{Spearman} = -0.18$ and probability of $P = 0.16$, so there appears to be no correlation. Our results do not confirm a correlation between radio loudness and black hole mass. When only the galaxies with $\text{FWHM}(H\beta) < 2000 \text{ km s}^{-1}$ are considered, the result is $\rho_{Spearman} = -0.262$, $P = 0.076$. This is still a fairly weak correlation.

NLS1 galaxies appear at the high Eddington ratio, low accretion rate extreme of the PC1-PC2 diagram. According to this model, NLS1 galaxies have small black hole masses and are radio quiet (Boroson 2002). We find that while it is still probable that NLS1 galaxies are in general radio quiet, they can have significant radio emission and can be radio loud. We also find that in general, the central black hole mass for an NLS1 galaxy is smaller than the typical AGN.

8.1. Test for Radio Loud/Radio Quiet Dichotomy

We wish to investigate what may be unusual about our radio loud NLS1 galaxies, to look for trends that could define what is different between radio loud NLS1 and radio quiet NLS1 galaxies. As has been shown by White et al. (2000), there is no radio loud- radio quiet dichotomy present in the FBQS. That property holds in the $\log R^*$ distribution of this sample of NLS1 galaxies, which, like the FBQS study as a whole, has its peak in the radio intermediate range. We run Student’s t-test on the various parameters in our sample and look for differences between radio loud and radio quiet samples. One of our results is shown Figure 20. In this figure is shown the distribution of the $[\text{OIII}]\lambda 5007/H\beta$ ratio, which for NLS1 galaxies is defined to be less than three. The two distribution are $\log R^* < 1$ (radio intermediate to radio quiet) in the upper panel and $\log R^* \geq 1$ (radio loud) in the lower panel. The shaded portions represent the galaxies with $\text{FWHM}(H\beta) < 2000 \text{ km s}^{-1}$ while the open portions are the $\text{FWHM}(H\beta) \geq 2000 \text{ km s}^{-1}$. The radio loud objects appear to be more heavily weighted towards the high $[\text{OIII}]$ -low $H\beta$ end of the ratio, while the radio quiet objects appear to be dominated by larger $H\beta$ flux. The radio loud sample does appear to be somewhat different from the radio quiet.

Student’s t-test provides a more stringent test of whether or not two sets of data differ significantly. When the test is performed on $[\text{OIII}]/H\beta$ ratio data, separated into $\log R^* \geq 1$ and $\log R^* < 1$, it suggests that for the NLS1 galaxies (44 total, due to 3 missing $[\text{OIII}]$ lines) the radio loud and radio quiet data sets may very well be two different populations. The result is $t = 2.40$ and probability that the difference is due to chance is 0.021. A similar result is present in the radio luminosity L_{20cm} ($t = 3.53$, $P = 0.01$). The result for radio luminosity strongly suggests two different populations, but that is not unusual, as a separation between radio loud and radio quiet should produce two populations in radio measurements.

Performing Student’s t-test in a similar manner on the FeII strength data we get ($t = 0.07$, $P = 0.95$), meaning that the radio loud and radio quiet populations are likely the same. A similar result holds for both the $\text{EW}(H\beta)$ measurements ($t = 0.829$, $P = 0.41$) and $\text{FWHM}(H\beta)$ ($t = 0.64$, $P = 0.50$). Again, there is no significant difference between the radio loud and radio quiet populations.

These galaxies are probably not a new class of AGN, but simply a group of regular NLS1 galaxies. However, they are significantly more luminous in the radio than those found previously and have greater [OIII] emission.

9. Summary

In this paper we presented the optical and radio properties of a sample of radio selected Narrow-line Seyfert 1 galaxies. We find 16 new radio loud NLS1 galaxies to add to the three that were previously discovered to increase the number of known radio loud NLS1 galaxies significantly. We have run Spearman rank correlation tests between several sets of parameters and find that, for the most part, our results agree with previous studies of NLS1 galaxies. When compared with X-ray selected and optically selected samples of NLS1 galaxies, the properties of radio-selected NLS1 galaxies do not exhibit many obvious differences from NLS1 galaxy samples selected in other manners. We also use Student’s t-test to determine whether radio loud NLS1 galaxies are statistically different from their radio quiet counterparts and conclude that there are few differences.

We estimate black hole masses with a relationship between $\text{FWHM}(\text{H}\beta)$, optical luminosity, and M_{BH} . We also estimate bulge velocity dispersion from $\text{FWHM}([\text{OIII}])$ and find that NLS1 galaxies do not obey the tight correlation between bulge mass and black hole mass, confirming the result of Grupe & Mathur (2004). Our sample seems to agree with the canonical model of NLS1 galaxies, in that they have small black hole masses and are accreting near the Eddington rate.

We have found a few discrepancies between our sample and previous studies of NLS1 galaxies and other AGN. We have found an anti-correlation between black hole mass and radio loudness showing that as M_{BH} increases, $\log R^*$ decreases. In previous studies of AGN, it has been found that radio loudness should increase as black hole mass increases. We test several correlations from Grupe et al. (1999) and Boroson (2002) and find that, while many of the properties in our sample agree with theirs, there are a few exceptions. We do not find an anti-correlation between the strength of FeII and [OIII], nor do we find any connection between $\text{FWHM}(\text{H}\beta)$ and $\text{EW}([\text{OIII}])$.

The most significant result found in this study is that we may now have to consider that NLS1 galaxies can be strong radio emitters. Although the galaxies in this study do not show the prodigious radio luminosities of radio loud quasars, the luminosities we find are significantly greater than the typical Seyfert galaxy.

Our sample of radio selected NLS1 galaxies adds significantly to the total of published NLS1 galaxies. Further investigation into this growing class of radio loud NLS1 galaxies could help define what is different physically between NLS1 and traditional Seyfert 1 galaxies. The authors are involved in a study of the X-ray properties of the most radio luminous objects in this sample, which we hope will reveal what is physically different about these NLS1 galaxies.

This work was partly performed under the auspices of the US Department of Energy, National Nuclear Security Administration by the University of California, Lawrence Livermore National Laboratory under contract No. W-7405-Eng-48

REFERENCES

- Antonucci, R. R. J., 1993, *ARA&A*, 31, 473
- Becker, R. H., White, R. L., Helfand, D. J., 1995, *ApJ*, 450, 559
- Bian, W., Zhao, Y., 2004, *MNRAS*, 343, 164
- Boller, Th., 1997, *AN*, 318, 209B
- Boller, Th., Brandt, W.N., Fink, H., 1996, *A&A*, 305, 53
- Boroson, T. A., 2003, *ApJ*, 585, 647
- Boroson, T. A., 2002, *ApJ*, 565, 78
- Boroson, T. A., Green, R. F., 1992, *ApJS*, 80, 109
- Brandt, W. N., Fabian, A. C., Nandra, K., Reynolds, C.S., Brinkmann, W. 1994, *MNRAS*, 271, 958B
- Brandt, W. N., Mathur, S., Elvis, M. 1997, *MNRAS*, 285, 25p
- Fabian, A. C., Rees, M. J., Stella, L., White, N. E., 1989, *MNRAS*, 238, 729
- Ferrarese, L., & Merrit, D. 2000, *ApJ*, 539, L9
- Gebhardt, K., et al. 2000, *ApJ*, 539, L13
- Gliozzi, M., Brinkmann, W., Laurent-Muehleisen, S. A., Moran, E. C., Whalen, J., 2001, *A&A*, 377, 44
- Goodrich, R. W., 1989, *ApJ*, 342, 224
- Gregg, M. D., Becker, R. H., White, R. L., et al. 1996, *AJ*, 112, 407
- Grupe, D., Mathur, S. 2004, *ApJ*, 606, L41
- Grupe, D., Leighly, K. M., Thomas, H. C., & Laurent-Muehleisen, S. A. 2000, *A&A*, 356, 11
- Grupe, D., Beuermann, K., Mannheim, K., Thomas, H.-C., 1999, *A&A*, 350, 805
- Haardt, F., and Maraschi, L., 1993, *ApJ*, 413, 507

- Ho, L. C., Peng, C. Y., 2001, *ApJ*, 555, 650
- Kaspi, S., et al. 2000, *ApJ*, 533, 631
- Laor, A., Fiore, F., Elvis, M., Wilkes, B. J., McDowell, J. C., 1997, *ApJ*, 477,93
- Leighly, K.M., 1999, *ApJS*, 125, 297L
- Leighly, K.M., 1998, *ApJS*, 125, 317L
- Madau, P., 1998, *ApJ*, 327, 116
- Mathur, S., Kuraszkiewicz, J., & Czerny, B. 2001, *New Astronomy*, 6, 321
- Mathur, S. 2000, *MNRAS*, 314, L17
- McLure, R. J., Dunlop, J. S., 2002, *MNRAS*, 331, 795
- Moran, E. C., Halpern, J.P., Helfand, D.J., 1996, *ApJS*, 106, 341
- Moran, E. C., Laurent-Muehleisen, S.A., Becker, R.H., et al., 2003, *ApJ*,(submitted)
- Oshlack, A. Y., Webster, R. L., Whiting, M. T., 2001, *ApJ*, 558, 578
- Osterbrock, D. E., Pogge, R.W., 1985, *ApJ*, 297, 166
- Pounds, K. A., Done,C., Osborne,J.P., 1995, *MNRAS*, 277, L5
- Puchnarewicz, E. M., et al. 1992, *MNRAS*, 256, 589
- Remillard, R. A., Bradt, H. V., Buckley, D. A. H., Roberts, W., Schwartz, D. A., Tuohy, I. R., & Wood, K. 1986, *ApJ*, 301, 742
- Schmidt, M. 1968, *ApJ*, 151, 393
- Siebert, J., Leighly, K. M., Laurent-Muehleisen, S. A., et al., 1999, *A&A*, 348, 678
- Sramek, R. A., Weedman, D. W. 1980, *ApJ*, 238, 435
- Stocke J. T., Morris S.L., Weymann R.J., Foltz, C.B., 1992, *ApJ*, 396, 487S
- Tremaine, S., et al. 2002, *ApJ*, 574, 740
- Ulvestad J. S., Antonucci, R., Goodrich, R.W., 1995, *AJ*, 109, 81
- Veron-Cerry, M. P., Veron, P., Goncalves, A. C., 2001, *A&A*, 372, 730
- White, R. L., Becker, R. H., Gregg, M.D., et al. 2000, *ApJS*, 126, 133
- Wills, D., Lynds, R. 1978, *ApJS*, 36, 317

Zhou, Hong-Yan, Wang, Ting-Gui, Dong, Xiao-Bo, Zhou, You-Yuan, and Li, Cheng, 2003,ApJ,
584, 147

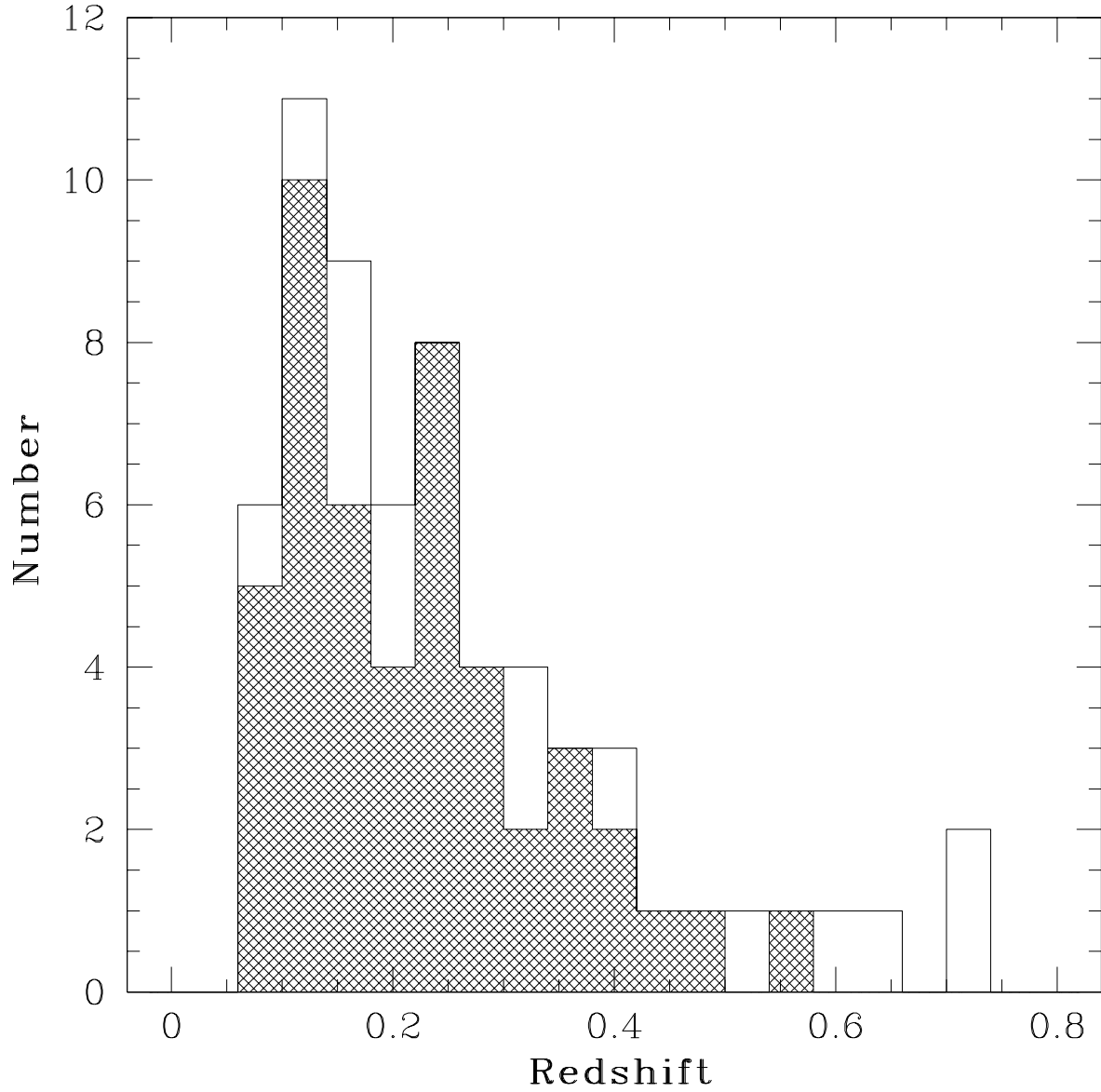


Fig. 1.— The distribution of redshifts for our sample of FBQS NLS1s. The shaded region represents the NLS1 galaxies while the other objects are BLS1 galaxies. Note the dearth of nearby NLS1s. This is due to FBQS selection criteria. If an object’s optical image was resolved, it was removed from the FBQS.

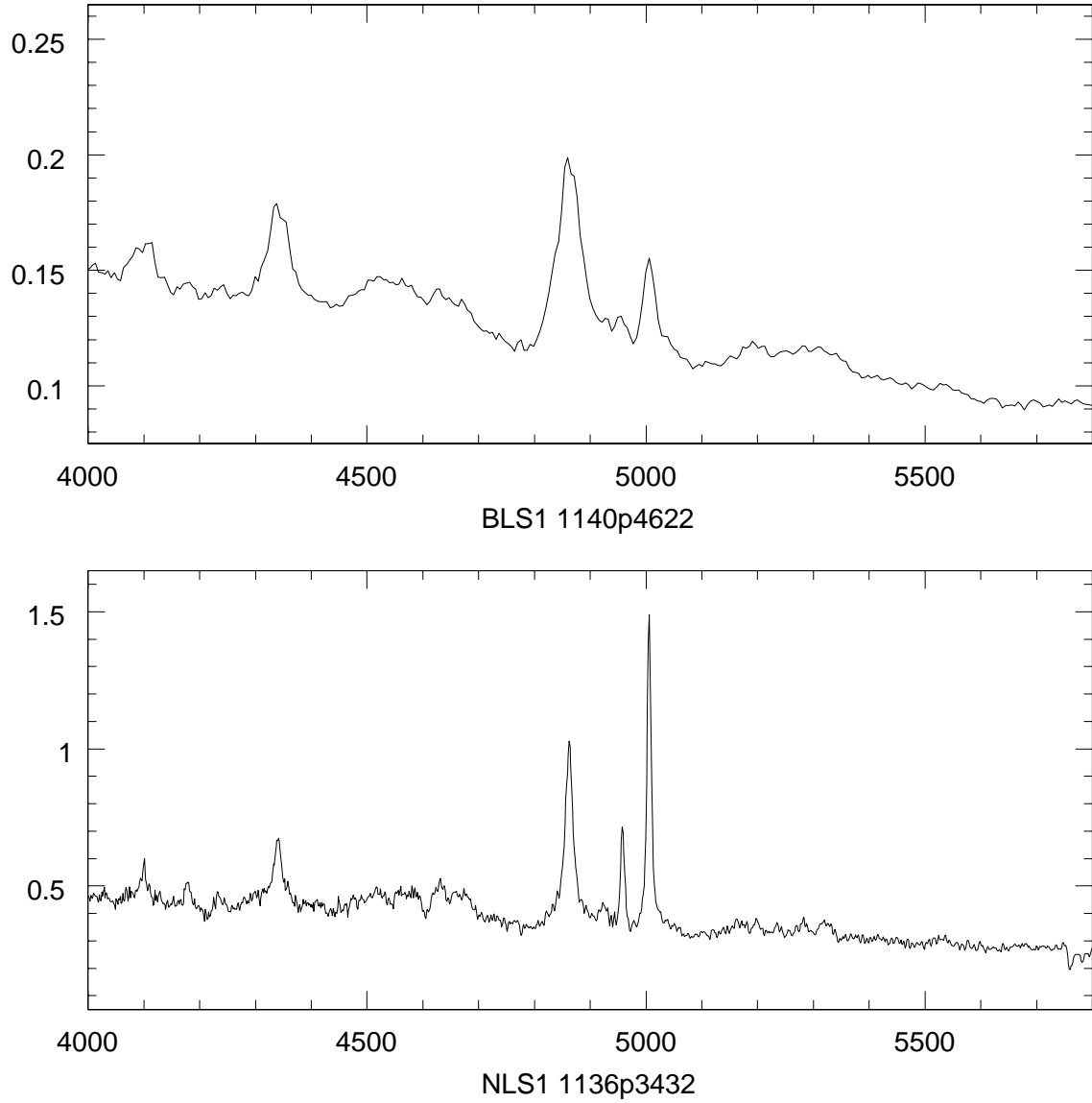


Fig. 2.— An example of an NLS1 and a BLS1. In the upper panel is 1140p4622 whose $\text{FWHM}(H\beta) = 2332 \text{ km s}^{-1}$ which qualifies as a standard Seyfert 1 galaxy (although on the narrow side). In the lower panel is 1136p3432 which has $\text{FWHM}(H\beta) = 918 \text{ km s}^{-1}$. The horizontal axis has units of angstroms and the vertical axis has units of $10^{-14} \text{ erg s}^{-1} \text{ cm}^{-2} \text{ \AA}^{-1}$.

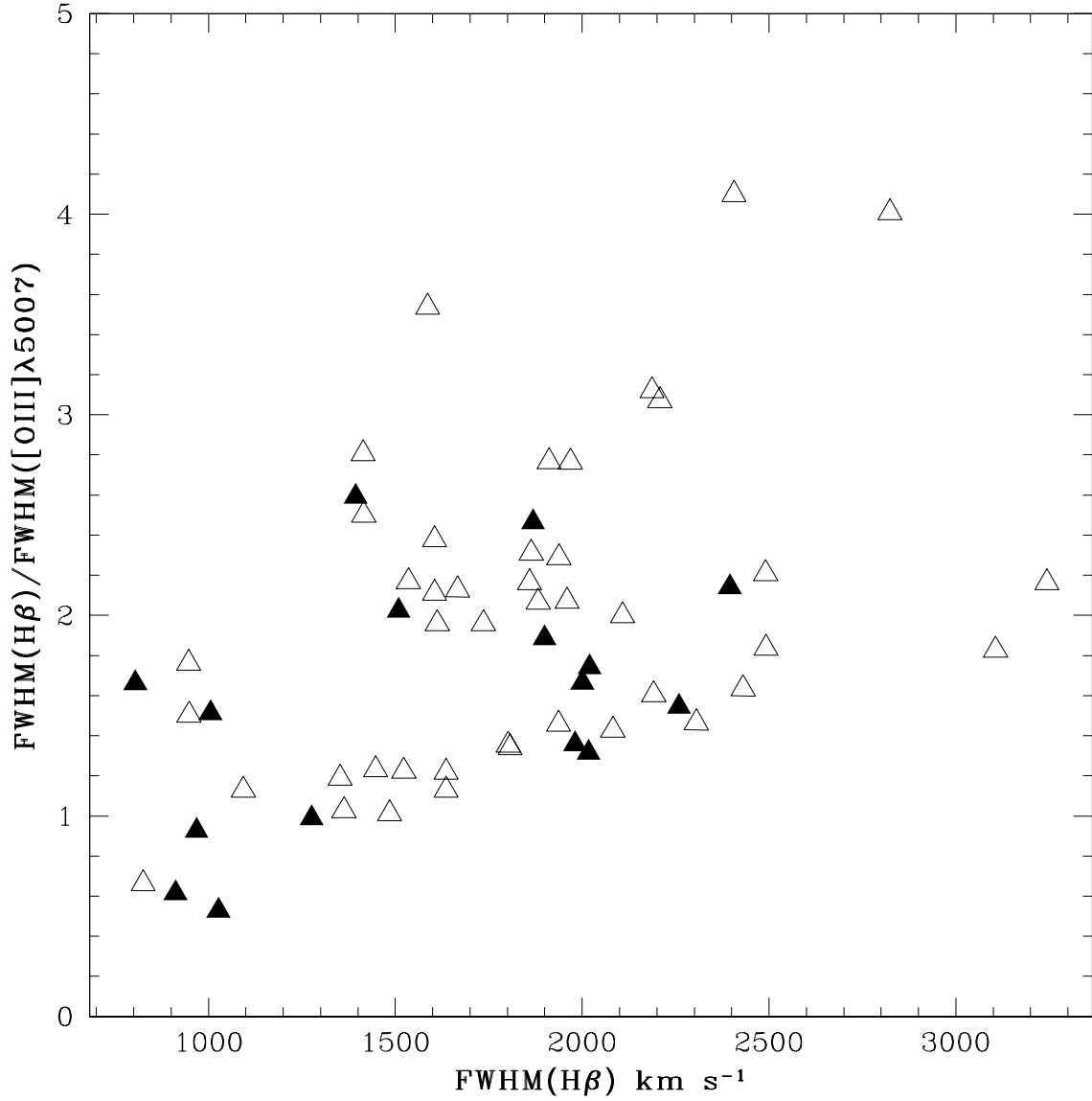


Fig. 3.— The ratio of $\text{FWHM}(\text{H}\beta)/\text{FWHM}([\text{OIII}]\lambda 5007)$ plotted against $\text{FWHM}(\text{H}\beta)$. Shaded triangles represent the radio loud objects, open triangles represent the radio quiet objects. As seen in the figure, the ratio for the objects with $\text{FWHM}(\text{H}\beta) > \sim 2000 \text{ km s}^{-1}$ are not statistically different from the traditional NLS1s with $\text{FWHM}(\text{H}\beta) < \sim 2000 \text{ km s}^{-1}$.

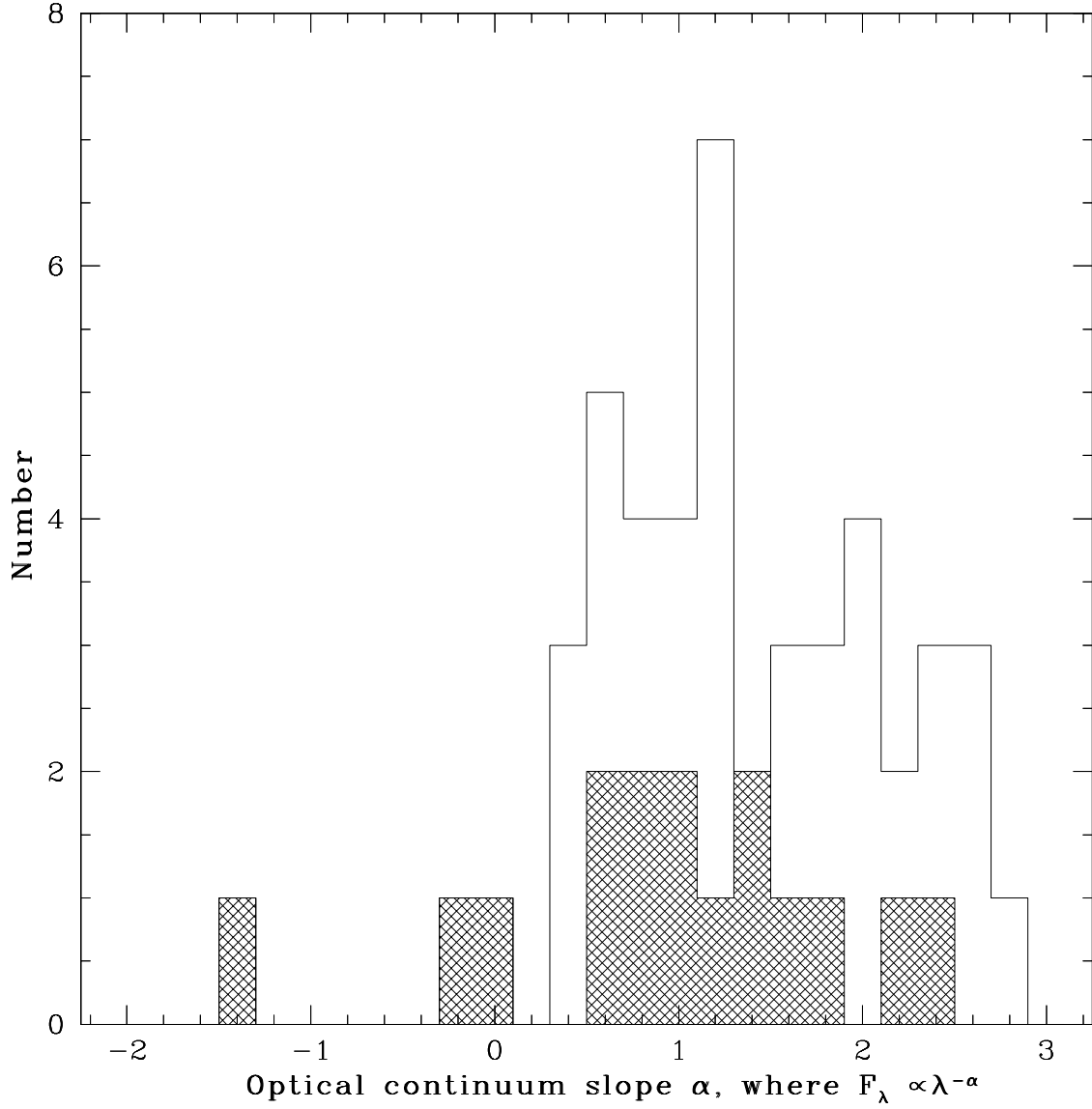


Fig. 4.— The distribution of the optical continuum slopes, α , for the continuum from 3000 Å to 7000 Å for the NLS1 galaxies only. The shaded region represents the radio loud distribution, the open region the radio quiet distribution. Spectra were fit with a powerlaw of the form $F_\lambda \propto \lambda^{-\alpha}$.

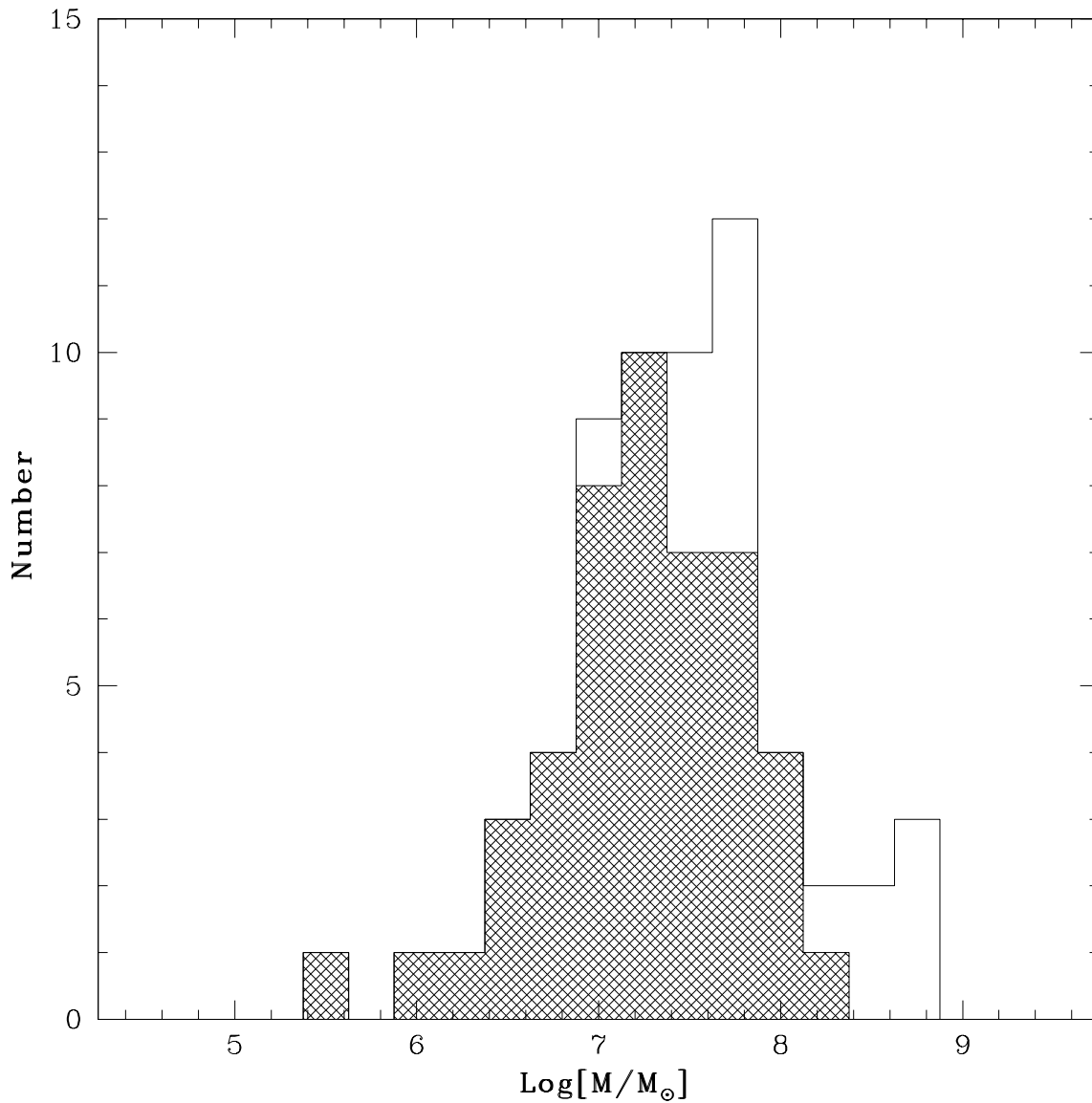


Fig. 5.— Estimated black hole mass distribution for all 62 objects in the sample using an empirical relation found by Kaspi et al. (2000). The masses are in units of solar masses. The shaded portion is the NLS1 galaxy distribution, the open region represents the BLS1 galaxy distribution.

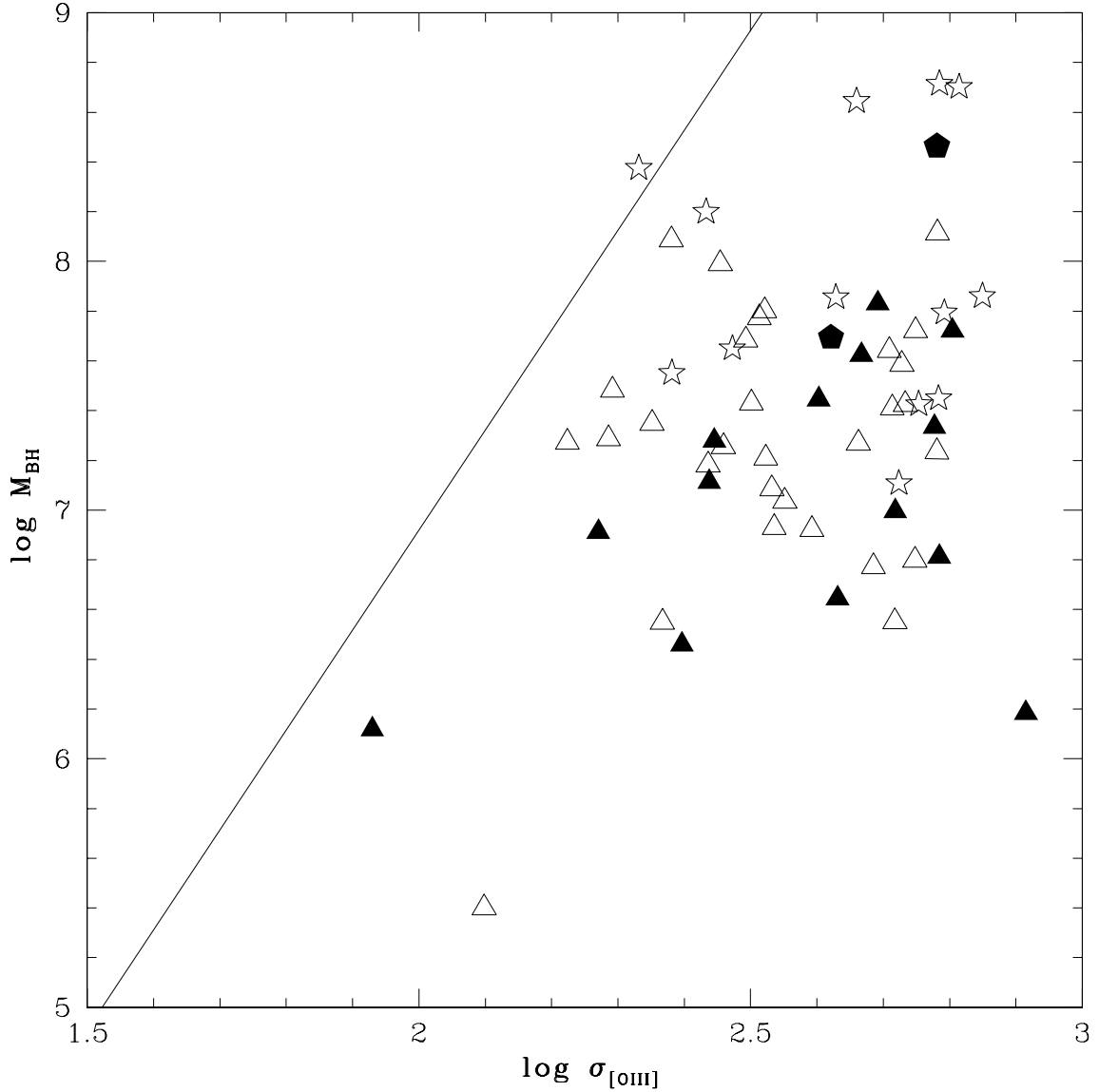


Fig. 6.— $M_{\text{BH}} - \sigma$ relation for 59 of the 62 objects in our sample. The open triangle are radio quiet NLS1s, filled triangles radio loud NLS1s, the stars are radio quiet BLS1, and the two filled pentagons represent radio loud BLS1s. The three missing objects have their $\lambda 5007$ lines destroyed by atmospheric absorption, and therefore were not included in this figure. The line is the relation found by Tremaine et al. (2002) for normal galaxies.

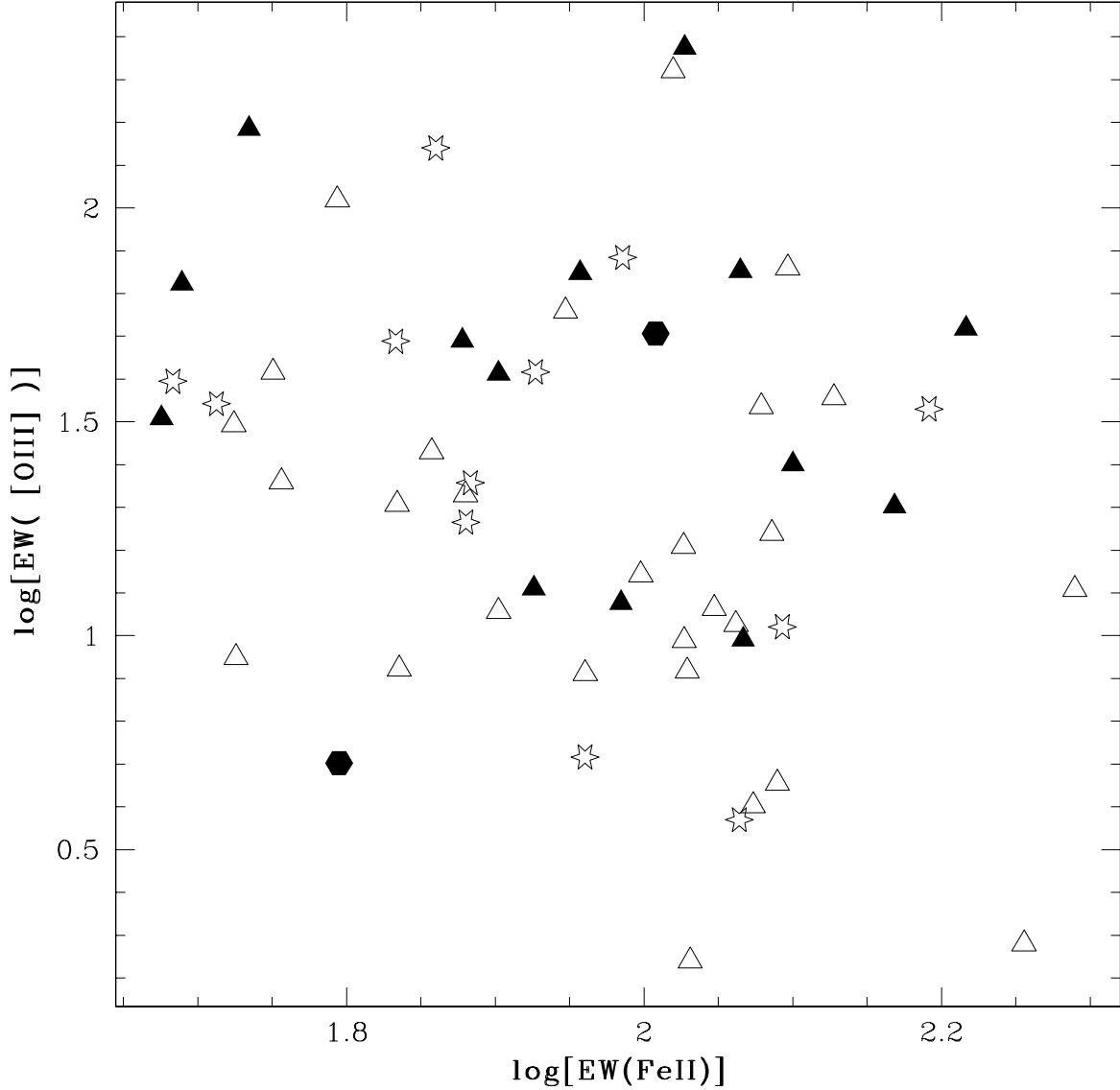


Fig. 7.— A plot of the FeII and [OIII] equivalent widths. Open triangles are radio quiet NLS1s, filled triangles are the radio loud NLS1s, open stars are radio quiet BLS1s, and the filled pentagons are radio loud BLS1s. When all 56 objects that have these measurements are considered, we find a relatively weak correlation, with $\rho_{Spearman} = -0.250$ and a probability of no correlation of 0.064. When only NLS1s are considered the probability of no correlation increases to 0.12. A correlation appears unlikely.

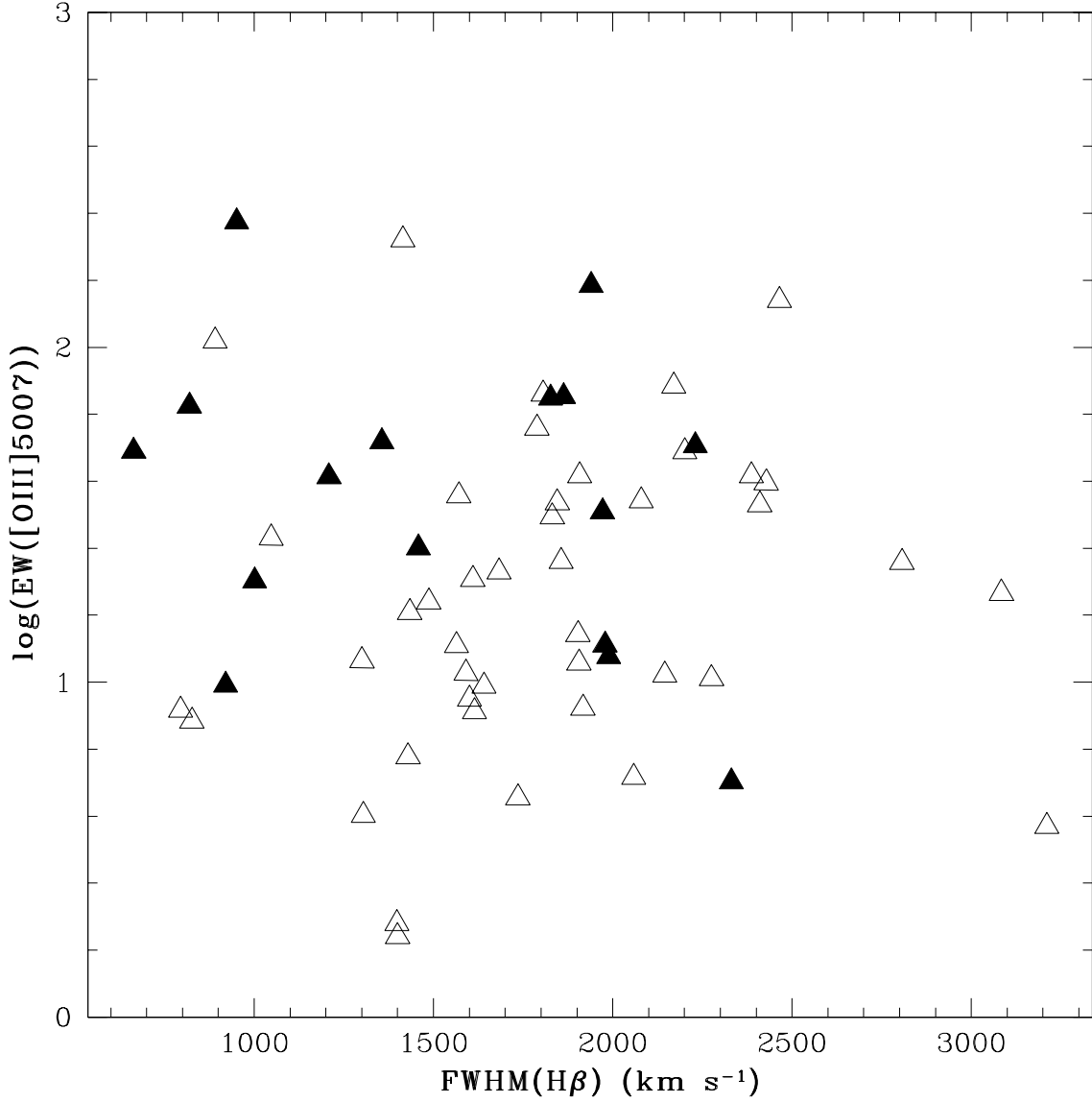


Fig. 8.— The equivalent width of $[\text{OIII}]\lambda 5007$ measured in \AA plotted against the FWHM of $\text{H}\beta$ in km s^{-1} . The open triangles represent NLS1 galaxies while the filled triangles represent the BLS1 galaxies. There is no correlation between these two parameters for the FBQS NLS1 galaxies. Spearman’s test gives a probability of chance correlation of $P = 0.73$.

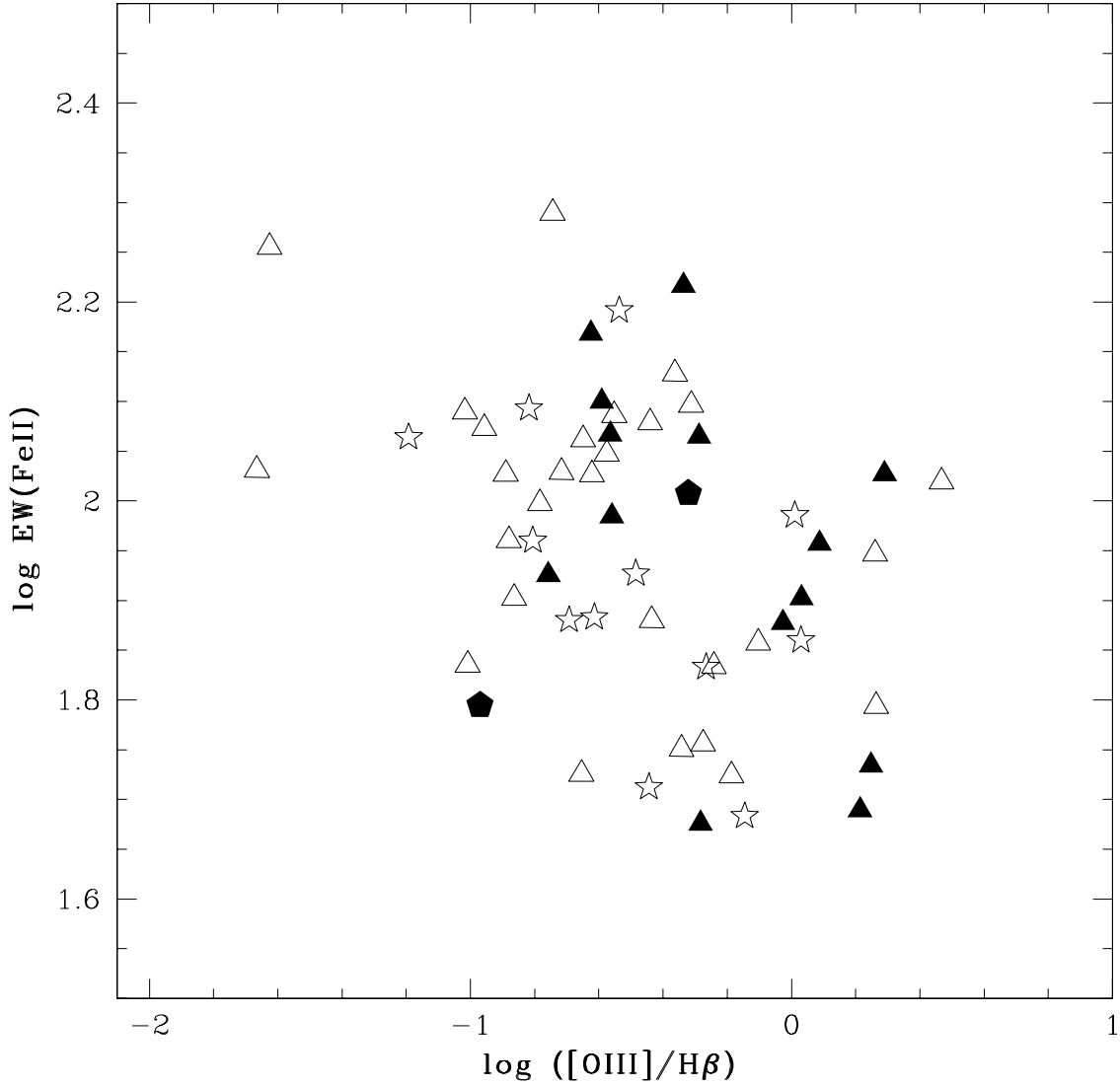


Fig. 9.— FeII equivalent widths plotted against $[OIII]/H\beta$ ratio. $EW(FeII)$ is measured in units of \AA . The open triangles are radio quiet NLS1 galaxies, the filled triangles radio loud NLS1 galaxies, the open stars are radio quiet BLS1 galaxies, and the filled pentagams are radio loud BLS1 galaxies. We integrated over two portions of each individual spectrum to get the FeII equivalent width. The details are in the text. The correlations are significant, with $\rho_{Spearman} = -0.419$, $P = 0.007$ for the NLS1s and $\rho_{Spearman} = -0.39$, $P = 0.004$ for the BLS1s.

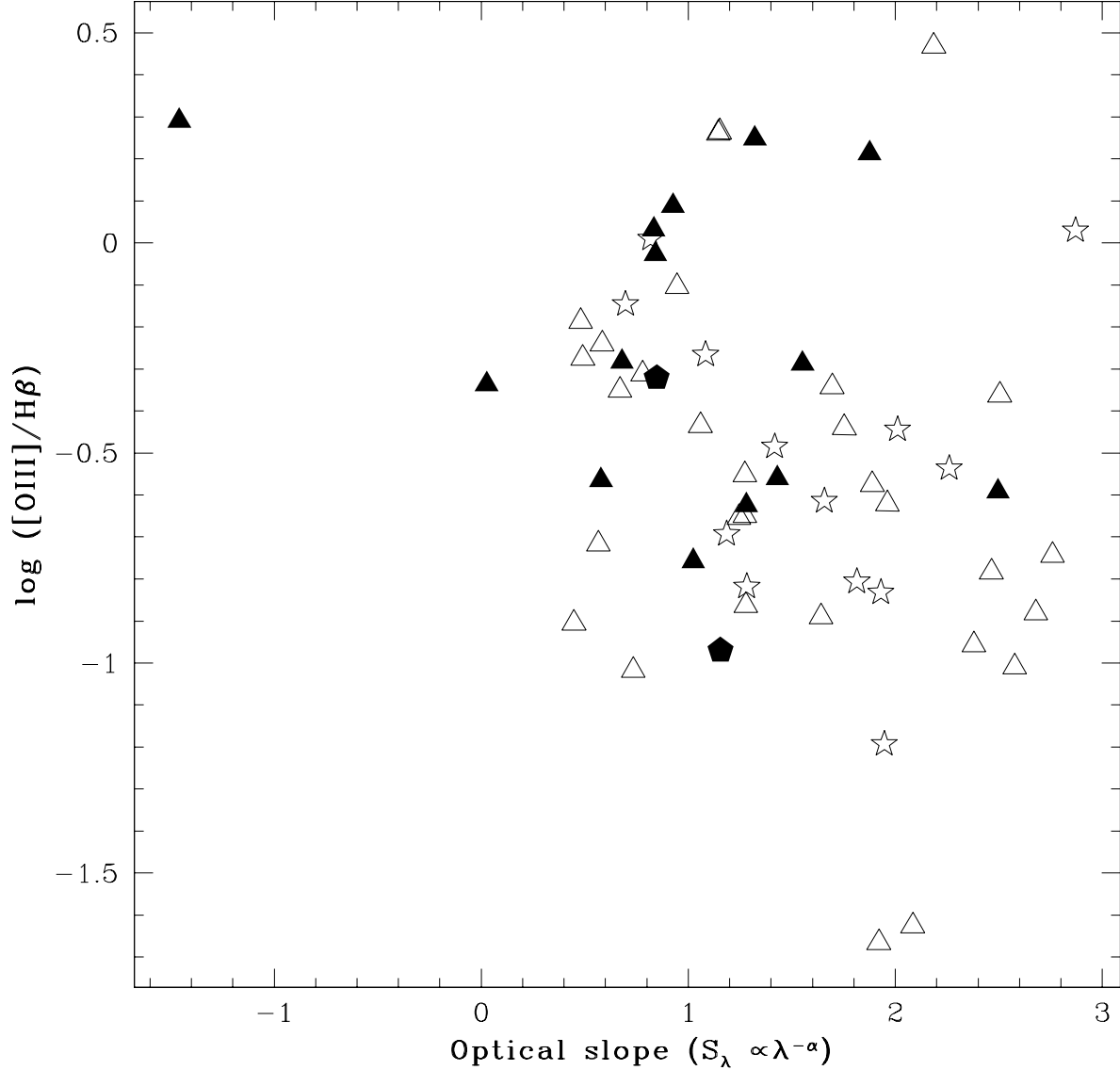


Fig. 10.— $[\text{OIII}]\lambda 5007/\text{H}\beta$ vs. optical slope α_{opt} . Open triangles represent radio quiet NLS1s, filled triangles for radio loud NLS1s, open stars for radio quiet BLS1s, and filled pentagams for radio loud BLS1s. This is for a slope measured between 3000 \AA and 7000 \AA . There is a statistically significant anti-correlation between optical slope and $[\text{OIII}]\lambda 5007/\text{H}\beta$ ratio with $\rho_{\text{Spearman}} = -0.345$ and probability of chance correlation of 0.009. There are only 59 data points as three of the objects have no $[\text{OIII}]\lambda 5007$ measurement.

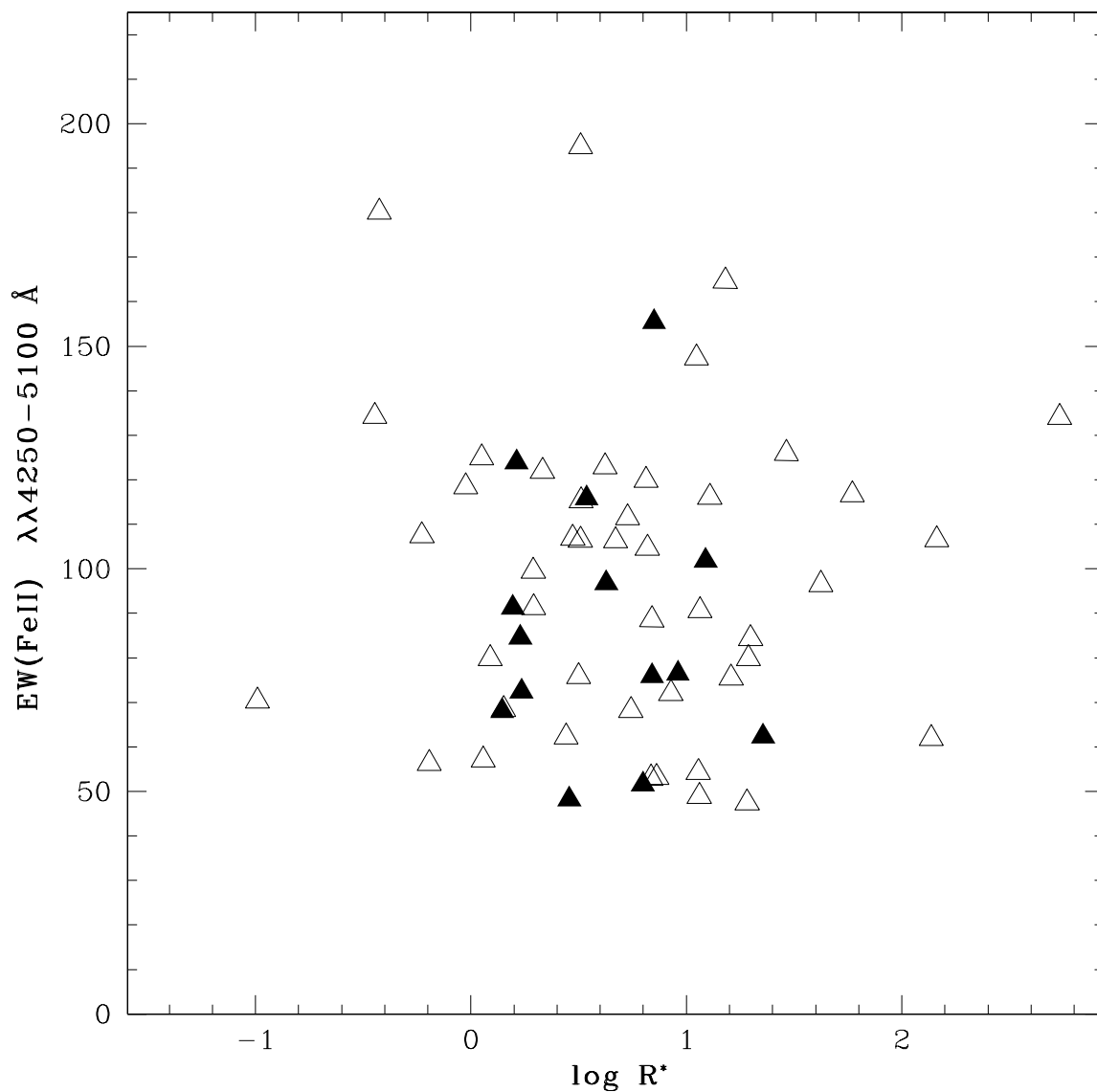


Fig. 11.— Radio loudness parameter $\log R^*$ and $\text{EW}(\text{FeII})$. Here the open triangles are NLS1 galaxies while the filled triangles are BLS1 galaxies. Boroson’s PCA analysis for a sample of 162 optically selected AGN suggested the possibility that FeII emission and radio loudness are linked. For the present collection of radio selected NLS1 galaxies, this does not appear to be true.

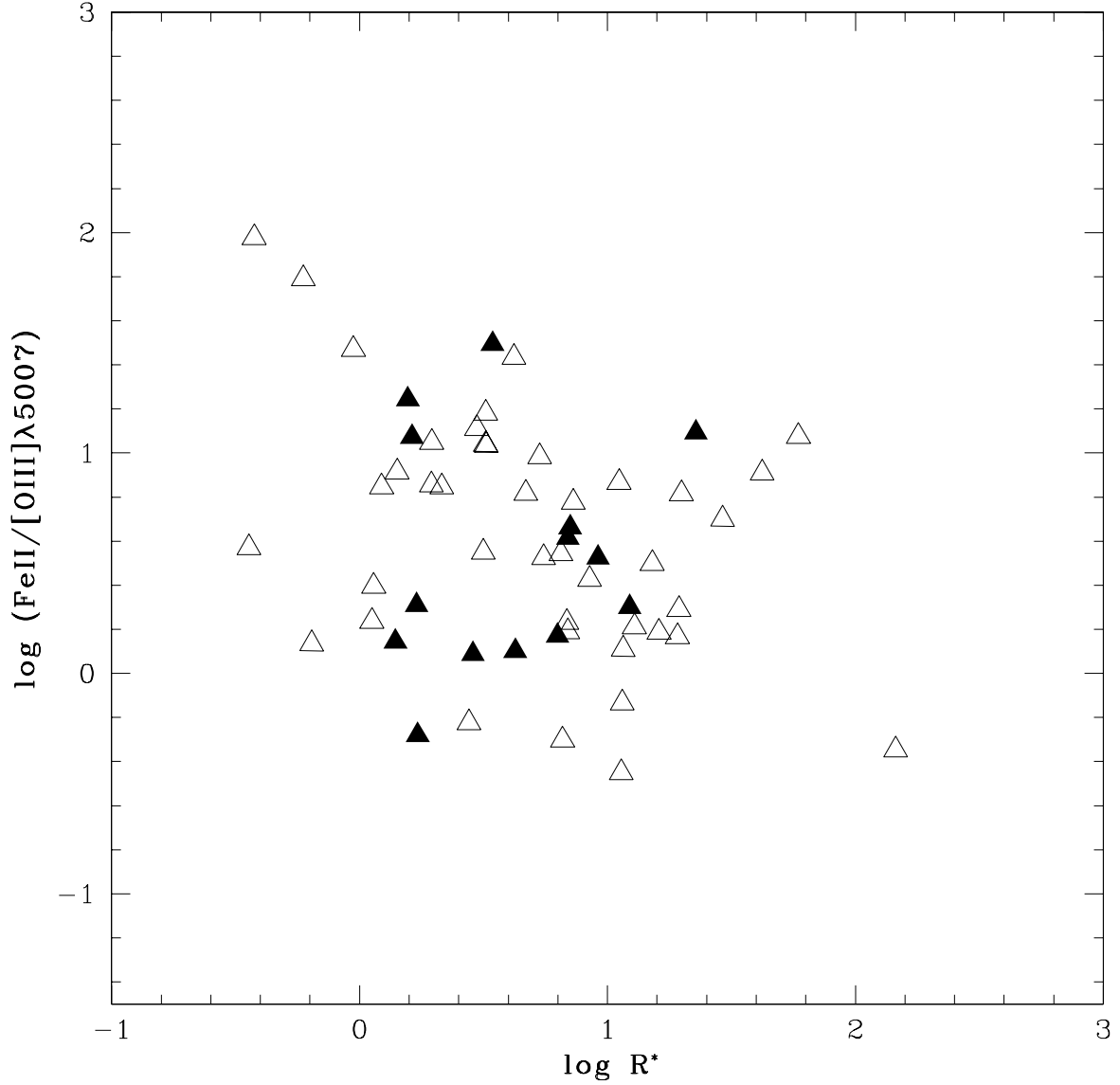


Fig. 12.— FeII/[OIII] ratio vs. $\log R^*$. The open triangles are NLS1 galaxies and the filled triangles are BLS1 galaxies. When only the NLS1s are considered, the correlation is significant, with $\rho_{\text{Spearman}} = -0.387$ and $P = 0.013$. When all 56 points are considered, the correlation is somewhat weaker with probability $P = 0.067$.

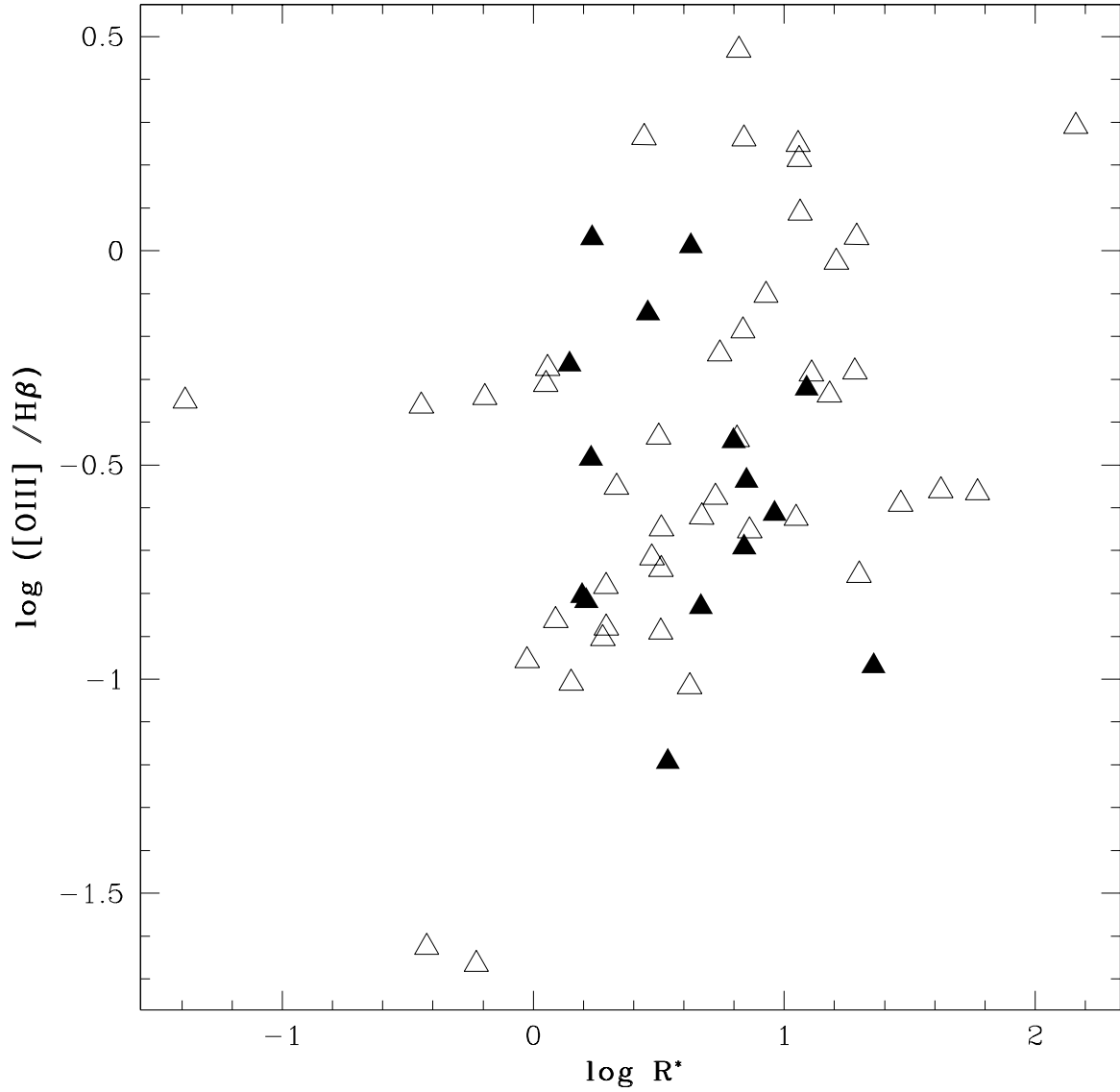


Fig. 13.— $[\text{OIII}]\lambda 5007/\text{H}\beta$ ratio plotted against radio loudness. The symbols are the same as in the previous figure, i.e, the filled triangles and NLS1 galaxies and open triangles are BLS1 galaxies. The Spearman rank correlation test reveals a possible correlation, $\rho_{\text{Spearman}} = 0.302$ and chance probability of 2%. When only NLS1 objects are considered, the correlation is even stronger with $\rho_{\text{Spearman}} = 0.442$ and probability $P = 0.004$

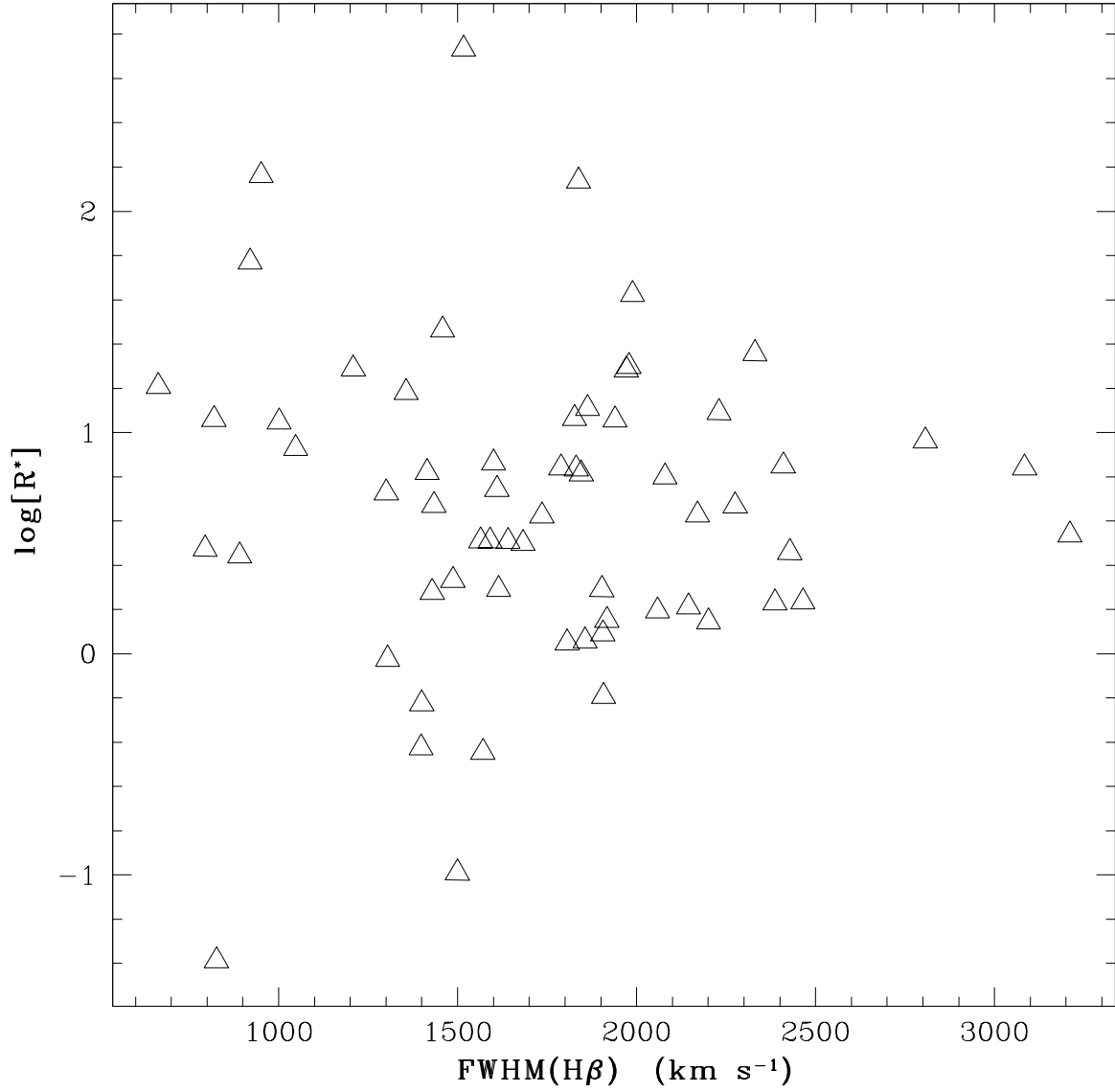


Fig. 14.— $\text{FWHM}(\text{H}\beta)$ (in km s^{-1}) vs. $\log R^*$ for the all 62 objects in this sample. There is no correlation evident and Spearman rank correlation tests confirm this with $\rho_{\text{Spearman}} = -0.046$ and $P = 0.72$ chance that this correlation could happen with random data.

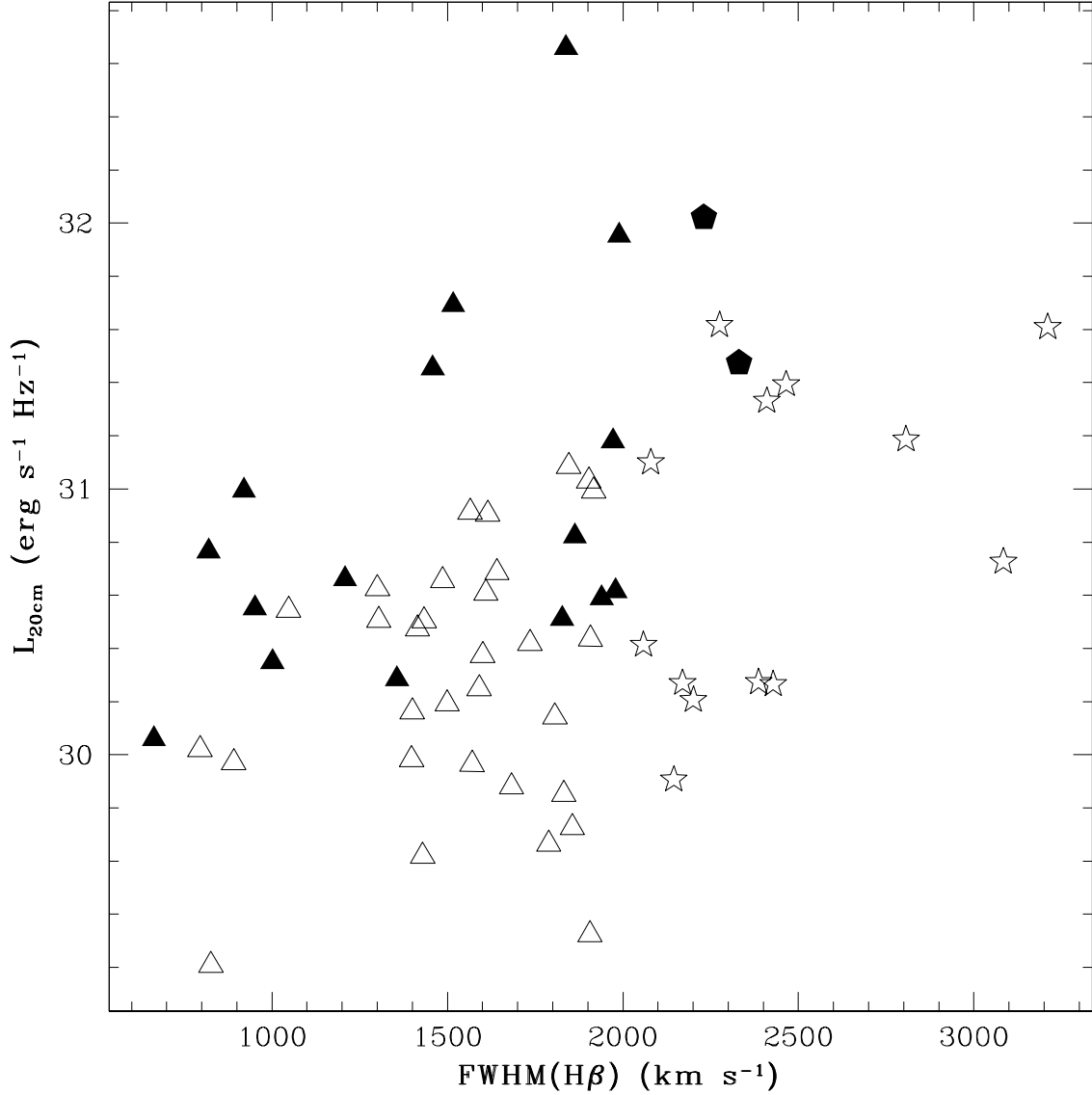


Fig. 15.— Twenty centimeter radio luminosity plotted against $\text{FWHM}(\text{H}\beta)$. The filled symbols are the radio loud objects while open symbols represent radio intermediate to radio quiet objects. Triangles represent NLS1 objects. The other symbols are BLS1 objects. There is a statistically significant correlation ($\rho_{\text{Spearman}} = 0.345$, $P = 0.007$) when all objects are considered. With only NLS1 objects considered, the correlation is weaker, with $\rho_{\text{Spearman}} = 0.246$ and probability $P = 0.095$. Vertical axis has units of $\text{erg s}^{-1} \text{Hz}^{-1}$ and the horizontal axis units of km s^{-1} .

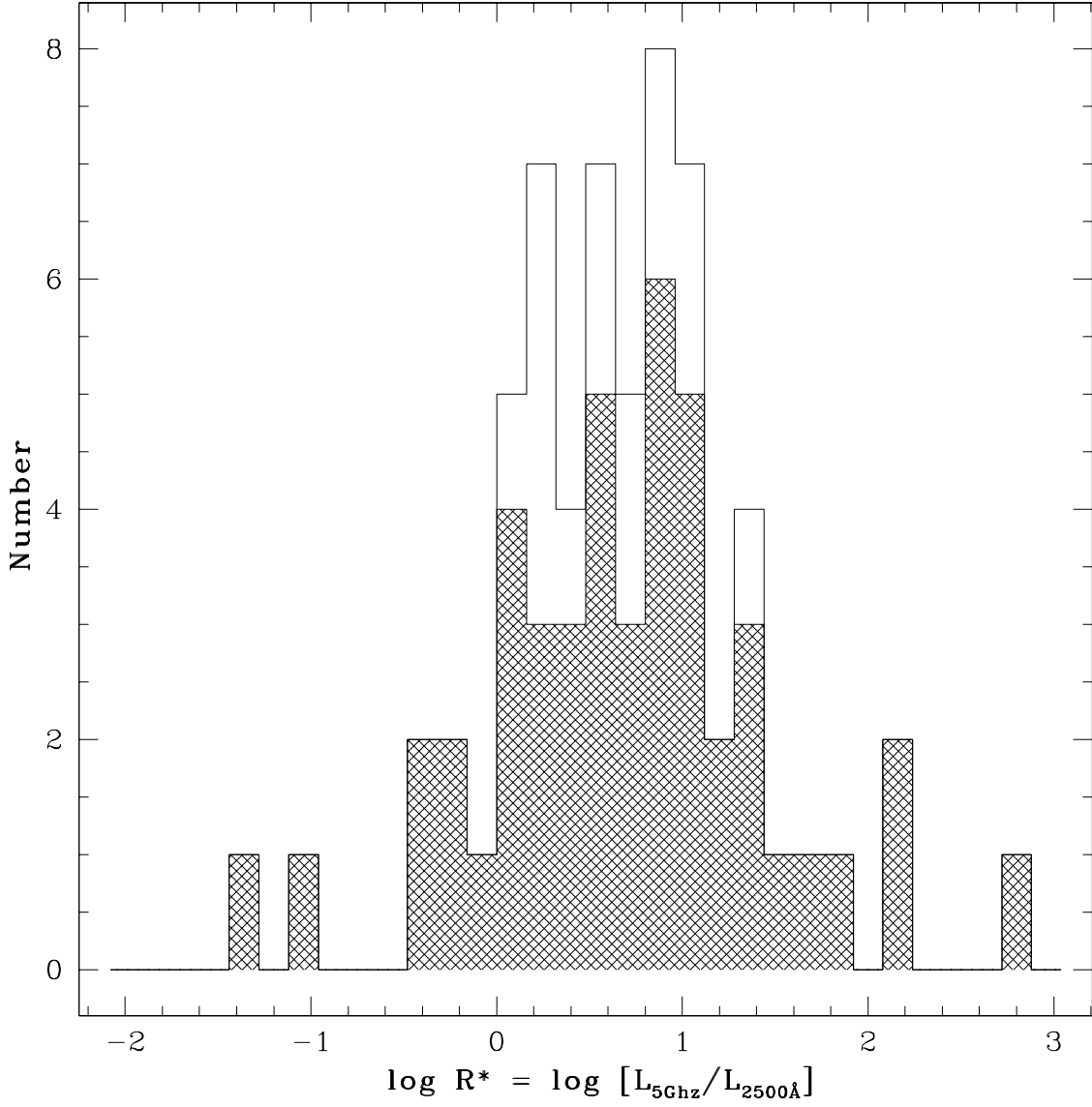


Fig. 16.— Distribution of radio loudness parameter, $\log R^*$, for all 62 objects in our sample. The shaded portion represents the NLS1 distribution and the open portion represents the BLS1 distribution. Our NLS1 distribution remarkably radio loud compared with previous samples of NLS1 galaxies.

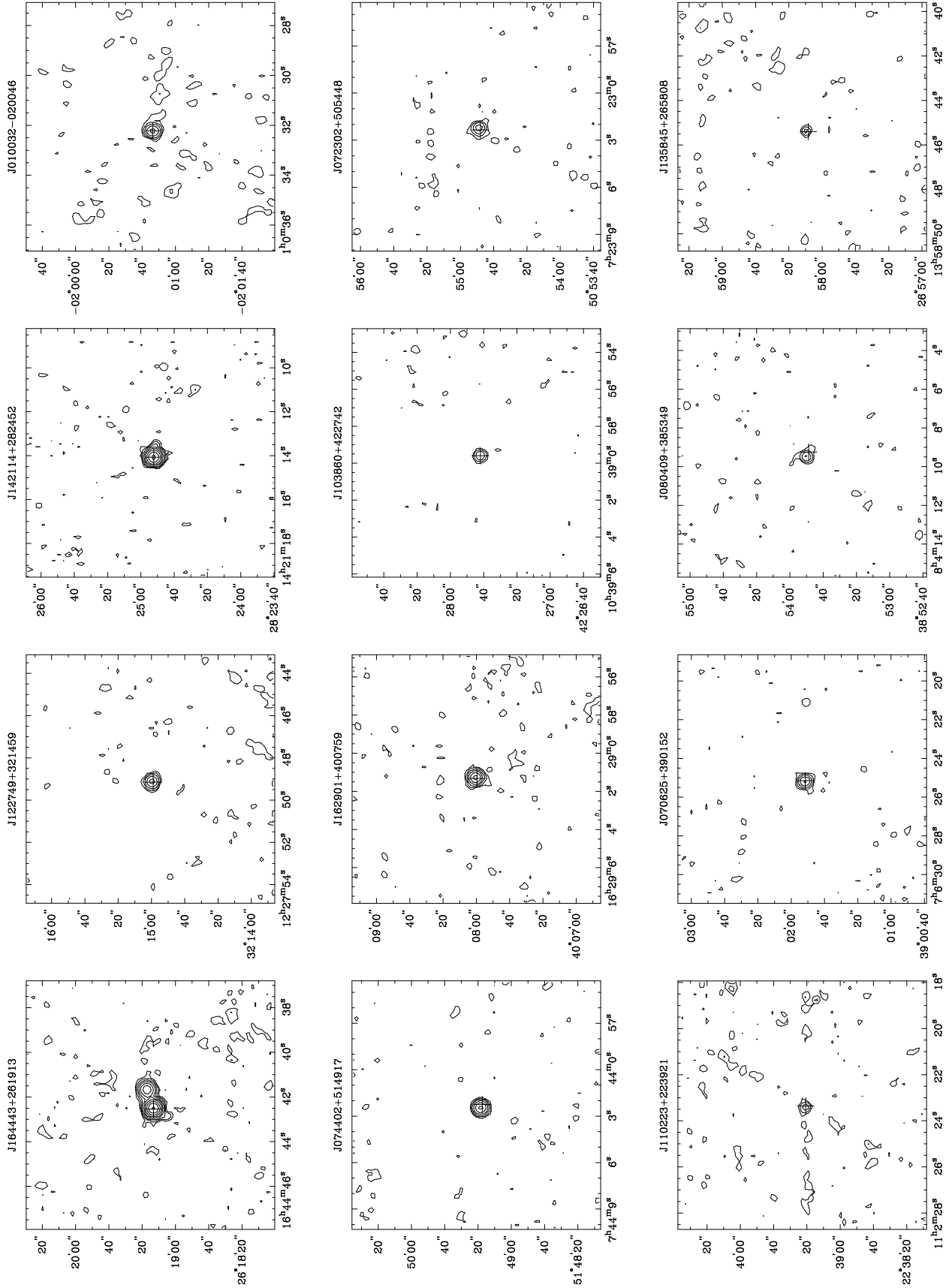


Fig. 17.— Twenty centimeter radio contours for the 12 radio loudest of the FBQS NLS1 galaxies. Note that there is no obvious structure most of the objects. They appear to be very compact,

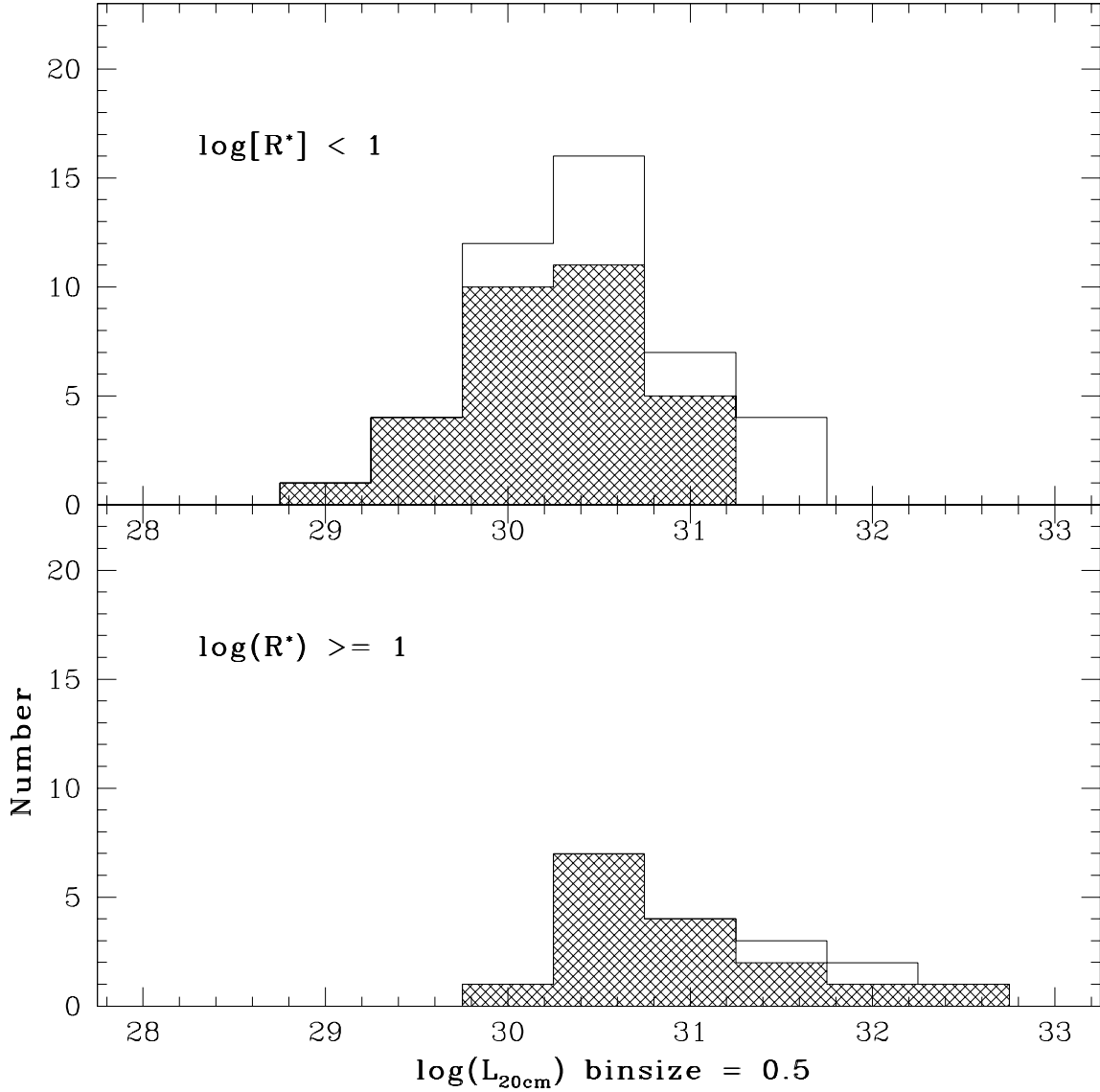


Fig. 18.— Distribution of 20 cm radio luminosities for our sample. The shaded portions represent the NLS1 galaxies and the open portion represents the BLS1 galaxies. The radio loud distribution is shown in the bottom graph, while $\log R^* < 1$ objects are on top.

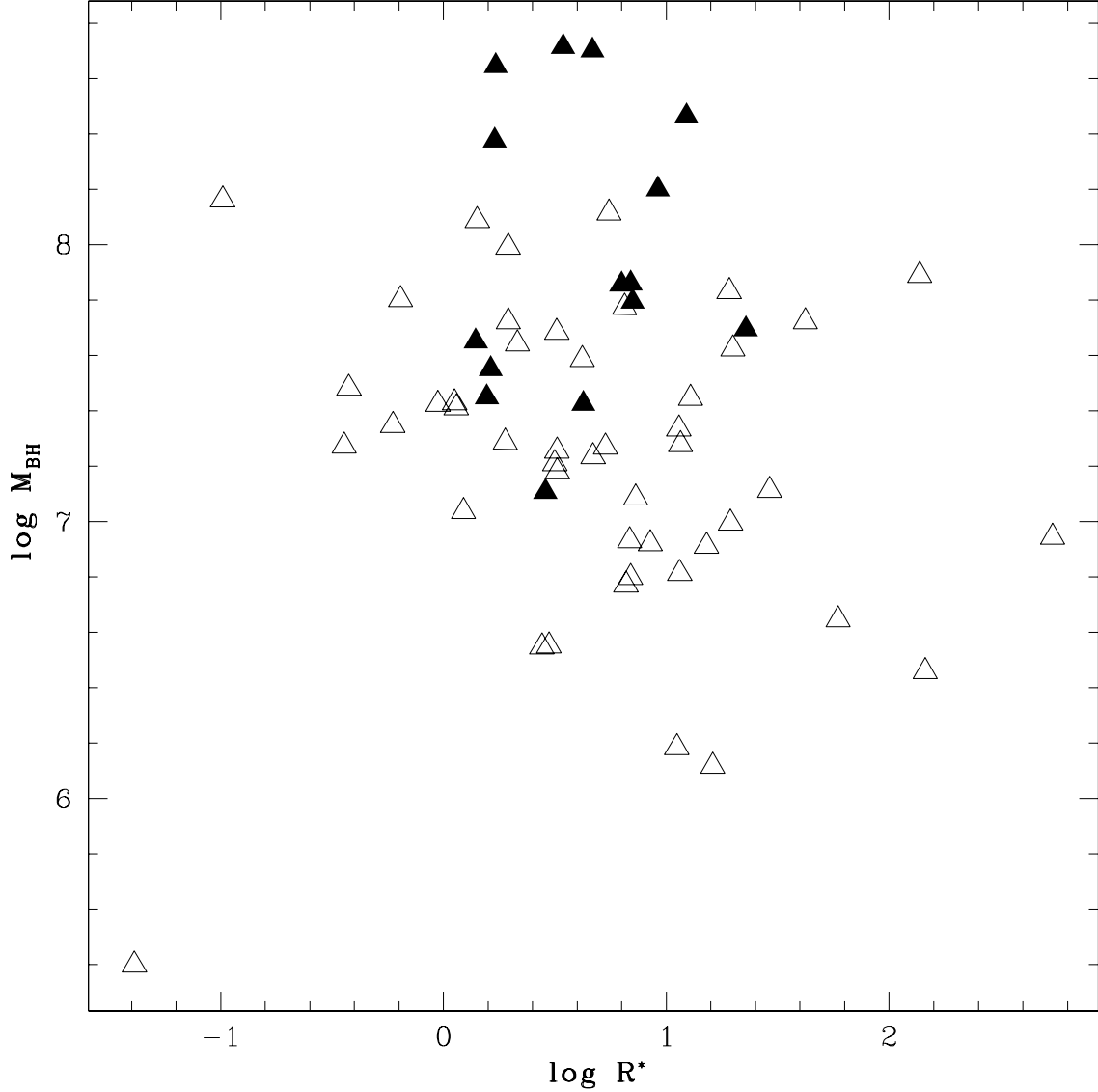


Fig. 19.— Plot of black hole mass vs. $\log R^*$. The open triangles are NLS1 galaxies and the filled triangles represent the BLS1 galaxies. The masses are given in units of solar mass. The correlation is not very compelling, with $\rho_{\text{Spearman}} = -0.18$ and the probability of chance correlation being $P = 0.16$ for all 62 objects in the sample. When considering just traditional NLS1 galaxies we get a stronger correlation ($\rho_{\text{Spearman}} = -0.262$, $P = 0.076$) but this is still not strong enough to get us tenure.

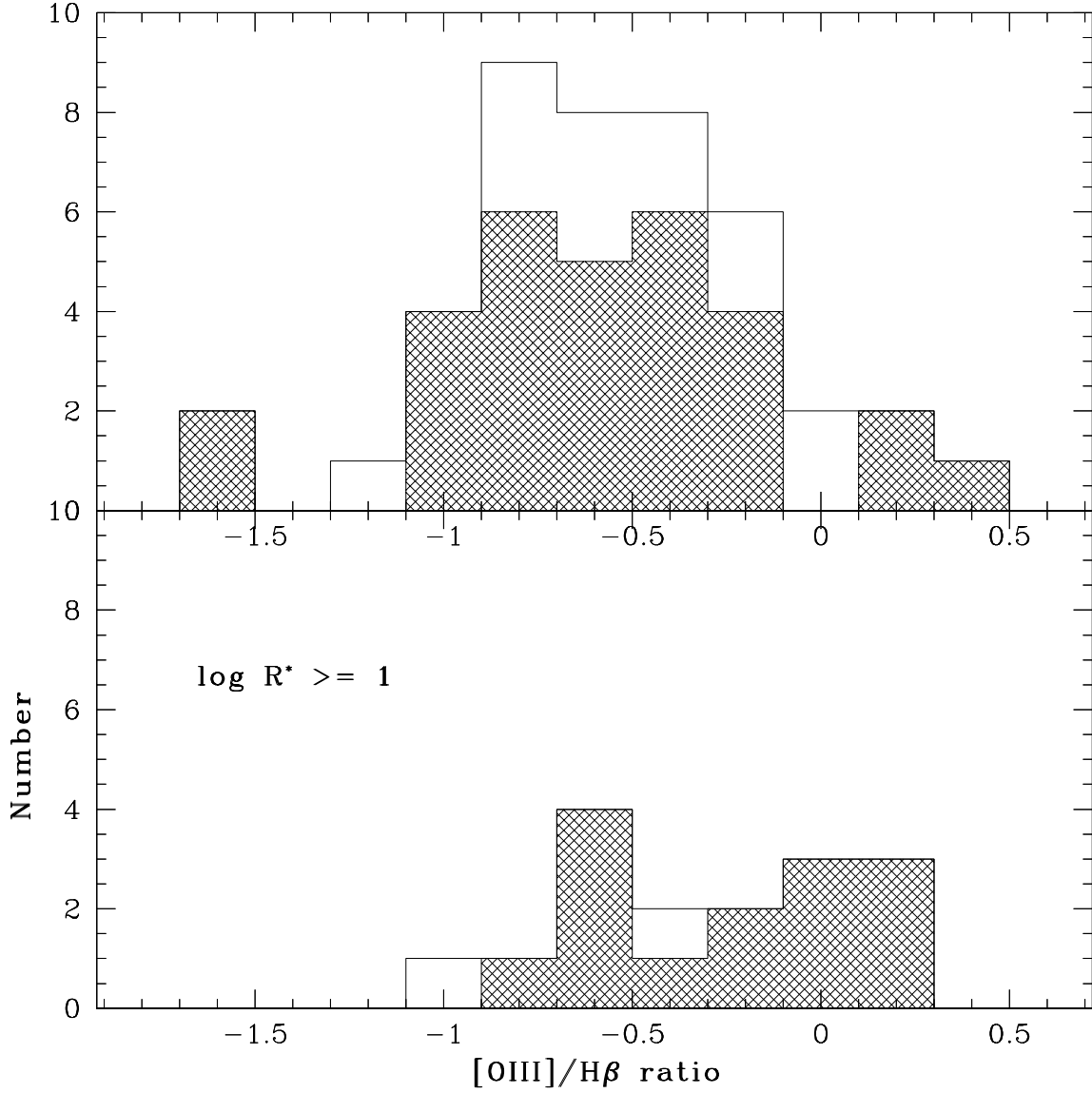


Fig. 20.— The distributions of $[OIII]/H\beta$ ratio separated into a radio loud and a radio quiet population. We additionally isolate the NLS1s and BLS1s, with the shaded region represents the NLS1 galaxies while the open region represents the BLS1 galaxies. The upper distribution is the radio quiet and the lower is radio loud. There are a total of 59 objects in the two distributions. Three objects with no $[OIII]$ measurements are not included.

Table 1. Spectrograph Characteristics

Telescope	Wavelength Range Å	Resolution Å
Lick 3 m	3600–8150	6
KPNO 2.1 m	3700–7400	4
APO 3.5 m	3650–10000	10
MMT 6 × 1.8 m	3600 – 8500	8
Keck II 10 m	3800–8800	8
ING 2.5 m	4870–8280	3.33

Table 2. NLS1 data.

Source	redshift	log R*	H β FWHM (km s $^{-1}$)	[OIII] λ 5007 FWHM (km s $^{-1}$)	[OIII]/H β	EW(FeII) $\lambda\lambda$ 4434-4684 \AA $\lambda\lambda$ 5147-5350 \AA	EW(H β) (\AA)	EW(OIII) (\AA)	slope (α) ($S_\lambda \propto \lambda^{-\alpha}$)
0022–1039	0.414	0.81	1845	766	0.363	119.9	89.8	34.3	1.75
0100–0200	0.227	1.77	920	1005	0.273	116.6	35.3	9.8	0.58
0706+3901	0.086	1.21	664	200	0.941	75.5	50.8	49.0	0.84
0713+3820	0.123	0.33	1487	1203	0.281	121.9	59.6	17.4	1.27
0721+4329	0.157	0.21	2145	565	0.152	123.9	66.4	10.5	1.28
0723+5054	0.203	1.29	1209	1228	1.074	79.8	37.3	41.0	0.83
0729+3046	0.147	0.44	891	547	1.836	62.2	54.9	104.4	1.15
0736+3926	0.118	0.05	1806	745	0.487	124.9	145.3	72.4	0.78
0744+5149	0.460	1.62	1989	1498	0.276	96.5	41.5	11.9	1.43
0747+4838	0.222	0.62	1735	1256	0.096	122.9	46.0	4.5	0.73
0752+2617	0.082	0.09	1906	837	0.137	79.8	80.2	11.4	1.28
0758+3920	0.095	–0.19	1908	780	0.455	56.3	86.5	41.4	1.69
0804+3853	0.151	1.18	1356	438	0.461	164.6	113.3	52.2	0.03
0810+2341	0.133	0.84	1831	807	0.650	53.0	47.3	31.2	0.48
0818+3834	0.160	0.50	1683	784	0.367	75.8	56.3	21.3	1.06
0833+5124	0.590	0.96	2806	637	0.243	76.4	89.2	22.8	1.66
0909+3124	0.265	0.74	1610	1422	0.574	68.2	34.7	20.3	0.58
0918+3024	0.538	0.85	2410	1455	0.291	155.5	109.1	33.9	2.26
0937+3615	0.180	0.93	1048	919	0.788	72.0	33.2	26.9	0.95
0946+3223	0.405	0.29	1615	1317	0.132	91.3	57.2	8.2	2.68
1005+4332	0.179	0.19	2059	1427	0.156	91.2	31.5	5.2	1.81
1010+3003	0.256	–0.02	1305	1272	0.111	118.4	33.8	4.0	2.38
1038+4227	0.220	1.30	1979	1091	0.175	84.3	71.6	12.9	1.02
1048+2222	0.329	0.73	1301	1080	0.266	111.5	41.3	11.6	1.89
1102+2239	0.455	1.28	1972	1155	0.522	47.4	60.6	32.2	0.68
1127+2654	0.379	0.29	1903	669	0.165	99.5	78.4	13.9	2.46
1136+3432	0.193	0.23	918	504	0.328	84.5	121.2	41.4	1.42
1140+4622	0.116	1.36	2331	982	0.107	62.3	45.4	5.0	1.16
1145+2906	0.142	0.14	2201	698	0.542	68.1	87.2	48.8	1.08
1151+3822	0.334	0.54	3210	1431	0.064	115.9	54.7	3.7	1.95
1157+2613	0.324	0.84	3084	1662	0.203	75.9	87.8	18.4	1.19
1159+2838	0.209	0.82	1415	1139	2.936	104.6	66.9	209.6	2.19
1220+3853	0.377	0.15	1917	564	0.098	68.4	79.1	8.4	2.58
1227+3214	0.137	2.16	951	585	1.951	106.5	126.8	236.9	–1.46
1256+3852	0.419	0.80	2079	999	0.360	51.6	91.3	34.9	2.01
1313+3753	0.655	0.68	2275	1533	0.155	...	62.7	10.1	1.94
1333+4141	0.225	1.06	1940	1407	1.770	54.2	83.2	153.2	1.32
1346+3121	0.246	0.86	1600	800	0.222	53.2	38.6	8.9	1.24
1358+2658	0.331	1.11	1863	941	0.515	116.1	132.3	71.3	1.55
1405+2555	0.165	–0.42	1398	460	0.024	180.1	75.6	1.9	2.08
1405+2657	0.713	1.09	2230	1419	0.477	101.8	103.9	50.9	0.85
1408+2409	0.131	0.51	1590	641	0.225	115.3	45.6	10.6	1.27
1421+2824	0.540	2.14	1838	61.9	52.2	...	2.18
1431+3416	0.715	0.23	2465	1073	1.071	72.4	118.4	138.1	2.87

Table 2—Continued

Source	redshift	log R*	H β FWHM (km s $^{-1}$)	[OIII] λ 5007 FWHM (km s $^{-1}$)	[OIII]/H β	EW(FeII) $\lambda\lambda$ 4434-4684 \AA $\lambda\lambda$ 5147-5350 \AA	EW(H β) (\AA)	EW(OIII) (\AA)	slope (α) ($S_\lambda \propto \lambda^{-\alpha}$)
1442+2623	0.108	0.47	795	1226	0.192	106.9	42.3	8.3	0.57
1448+3559	0.114	0.06	1856	1216	0.531	57.0	42.5	22.9	0.49
1517+2239	0.109	0.84	1789	1314	1.823	88.5	30.4	57.4	1.15
1517+2856	0.209	0.63	2170	1332	1.024	96.8	73.1	76.7	0.82
1519+2838	0.270	0.51	1641	731	0.129	106.4	72.0	9.7	1.64
1610+3303	0.098	0.46	2428	1243	0.715	48.2	53.9	39.3	0.70
1612+4219	0.233	1.06	819	1430	1.635	48.9	38.6	66.7	1.88
1629+4007	0.272	1.46	1458	643	0.256	125.9	91.2	25.2	2.50
1644+2619	0.145	2.73	1517	134.0	67.9	...	-0.11
1702+3247	0.164	-0.23	1400	528	0.022	107.4	76.0	1.7	1.92
1709+2348	0.254	1.06	1827	655	1.224	90.6	56.0	70.4	0.93
1713+3523	0.085	1.05	1002	1933	0.237	147.4	81.4	20.1	1.28
1716+3112	0.110	-0.45	1571	393	0.434	134.2	77.2	36.0	2.50
1718+3042	0.281	0.67	1434	1418	0.239	106.3	63.8	16.2	1.96
2155-0922	0.192	-0.99	1500	70.3	31.1	...	2.03
2159+0113	0.101	0.28	1429	454	0.124	...	47.4	6.0	0.45
2327-1023	0.065	-1.39	652	538	0.390	...	7.66	16.85	0.67
2338-0900	0.374	0.51	1564	676	0.180	194.8	65.7	12.8	2.76

Note. — Objects 1421+2824, 1644+2619, and 2155-0922 had [OIII] emission lines destroyed by atmospheric lines.